Journal of Natural Fibers

ISSN: 1544-0478 (Print) 1544-046X (Online) Journal homepage: www.tandfonline.com/journals/wjnf20

Forecasting the Thermal Degradation Depending on the Kinetics of *Dracaena Draco* Lignocellulosic Fibers Using an Artificial Neural Network

Abdelwaheb Hadou, Ahmed Belaadi, Djamel Ghernaout & Herbert Mukalazi

To cite this article: Abdelwaheb Hadou, Ahmed Belaadi, Djamel Ghernaout & Herbert Mukalazi (2025) Forecasting the Thermal Degradation Depending on the Kinetics of *Dracaena Draco* Lignocellulosic Fibers Using an Artificial Neural Network, Journal of Natural Fibers, 22:1, 2531368, DOI: 10.1080/15440478.2025.2531368

To link to this article: https://doi.org/10.1080/15440478.2025.2531368

JOURNAL OF NATURAL FIBERS
2025, VOL. 22, NO. 1, 2531368
https://doi.org/10.1080/15440478.2025.2531368

Taylor & Francis
Taylor & Francis Group

Forecasting the Thermal Degradation Depending on the Kinetics of *Dracaena Draco* Lignocellulosic Fibers Using an Artificial Neural Network

Abdelwaheb Hadou[a], Ahmed Belaadi[a], Djamel Ghernaout[b,c], and Herbert Mukalazi[d]

[a]Department of Mechanical Engineering, Faculty of Technology, University 20 August 1955- Skikda, Skikda, Algeria; [b]Chemical Engineering Department, College of Engineering, University of Ha'il, Ha'il, Saudi Arabia; [c]Chemical Engineering Department, Faculty of Engineering, University of Blida, Blida, Algeria; [d]Department of Mathematics and Statistics, Kyambogo University, Kampala, Uganda

ABSTRACT

In order to forecast the thermal degradation of *Dracaena draco* plant fibers (DDFs) using thermogravimetric analysis (TGA) at heating rates ranging from 5 to 30°C/min, this study employed artificial neural networks (ANNs). Hemicellulose, cellulose, and lignin breakdown were represented by the three different degradation stages that were seen. The enhanced ANN27 model successfully captured pyrolysis behavior and degradation patterns, achieving a high prediction accuracy ($R^2 = 0.99966$). The model performed well at lower heating rates (5 and 10°C/min), but because of bias and heteroscedasticity, adjustments are required at higher rates (15–30°C/min). In contrast to the experimental averages of 131.244 kJ/mol, 109.269 kJ/mol, and 131.694 kJ/mol, respectively, kinetic analysis showed that the ANN27-predicted activation energies (Ea) were 133.420 kJ/mol (KAS), 53.692 kJ/mol (FWO), and 133.784 kJ/mol (STR). Without requiring a lot of testing, our ANN method provides insights into DDF thermal behavior and optimizes processing settings by properly forecasting degradation curves.

摘要

为了使用热重分析（TGA）在5至30°C/min的加热速率下预测龙血树植物纤维（DDF）的热降解，本研究采用了人工神经网络（ANN）. 半纤维素、纤维素和木质素的分解由所看到的三个不同的降解阶段表示. 增强的ANN27模型成功捕获了热解行为和降解模式，实现了高预测精度（R2 = 0.99966）. 该模型在较低的加热速率（5和10°C/min）下表现良好，但由于偏差和异方差性，需要在较高的速率（15-30°C/min）下进行调整. 与实验平均值131.244 kJ/mol、109.269 kJ/mol和131.694 kJ/mol相比，动力学分析表明，ANN27预测的活化能（Ea）分别为133.420 kJ/mol（KAS）、53.692 kJ/mol. 在不需要大量测试的情况下，我们的ANN方法提供了对DDF热行为的见解，并通过正确预测降解曲线来优化处理设置.

KEYWORDS

Kinetic analyses; *Dracaena Draco* fiber; thermal properties; artificial neural networks; pyrolysis

关键词

动力学分析; Dracaena Draco维; 热性能; 人工神经网络; 热解

Introduction and literature review

The usage of biomass, particularly woody biomass, which accounts for over 90% of the annual energy produced from all biomass sources, has seen a significant increase since 2000, more than doubling the bioenergy consumed in terms of oil equivalents (Lazzari et al. 2019). The prominent role of biomass in Europe's energy mix underscores its critical importance in meeting current and future energy demands. Lignocellulosic materials, derived from wood and plant fibers, are sustainable resources with exceptional mechanical properties, high energy output, and renewability (Giridharan 2019). These attributes make lignocellulosic fibers a promising alternative to traditional petroleum-based materials in composite production, enabling the creation of stronger, lighter, and more environmentally friendly composites. These materials find applications in industries such as automotive, aerospace, and construction (Neves et al. 2019).

Beyond composites, lignocellulosic materials can serve as petroleum adsorbents, capable of absorbing hazardous hydrocarbons, thus offering potential solutions for cleaning up oil spill-related soil and water contamination. Additionally, through photosynthesis, plants capture CO2, storing it in their cells to

CONTACT Herbert Mukalazi hmukalazi@kyu.ac.ug Department of Mathematics and Statistics, Kyambogo University, Kampala, Uganda; Ahmed Belaadi a.belaadi@univ-skikda.dz; ahmedbelaadi1@yahoo.fr Department of Mechanical Engineering, Faculty of Technology, University 20 August 1955- Skikda, Skikda, El-Hadaiek, Algeria

mitigate the greenhouse effect, thereby playing a vital role in reducing CO2 emissions and combating climate change (Pang 2019; Proskurina et al. 2019).

Composed of hemicellulose, cellulose, and lignin, lignocellulosic materials possess a complex, anisotropic structure that significantly influences their thermal properties, including degradation and disintegration (Alongi and Malucelli 2015; Ornaghi et al. 2020). Factors such as density, moisture content, chemical composition, and crystallinity impact the kinetics of these reactions. Understanding these variables is essential for optimizing the use of lignocellulosic materials across various applications. For instance, pre-treatments that reduce moisture content or modify crystalline structure can enhance thermal stability (Castro, da Silva, and Virgens 2020; Zanchet et al. 2019).

Pyrolysis, the thermal degradation of plant fibers in the absence of oxygen, breaks down biomass components into renewable energy and chemical precursors (Lopes and Tannous 2020). The gases and char produced during pyrolysis can be used to create biofuels, chemicals, and other valuable resources, while the steam generated can produce heat or electricity (Vyazovkin 2020). Understanding pyrolysis mechanisms is crucial for optimizing product yields and operational efficiency. Kinetic and thermal models simulate plant fiber behavior during thermal degradation, providing valuable insights for pyrolysis reactor design and reducing the need for extensive experimental work (Bednaya and Konovalenko 2018).

Recent advancements in the study of thermal degradation mechanisms of lignocellulosic materials and polymers have provided deeper insights into their kinetics and degradation pathways, as evidenced by several key studies. For instance, Basak et al. (Basak et al. 2021) explored polymer degradation under diverse environmental conditions, shedding light on the factors influencing stability and decomposition (Basak et al. 2021). Similarly, Bhowmick et al. focused on the stability and kinetic parameters of polymer degradation, offering a detailed analysis of reaction mechanisms (Bhowmick, Basak, and Samanta 2022). Basak et al. (Basak and Ali 2022) further contributed by examining combustion and thermal degradation processes, emphasizing the role of chemical composition in degradation behavior (Basak and Ali 2022). Additionally, Alongi et al. provided a comprehensive analysis of degradation mechanisms in advanced materials, highlighting the applicability of their findings to lignocellulosic systems (Alongi et al. 2013). These studies collectively underscore the complexity of thermal degradation, driven by factors such as chemical structure, moisture content, and environmental conditions, necessitating advanced predictive tools to optimize material applications. Nasri and Toubal (Nasri and Toubal 2024) employed ANNs to predict tensile strength and impact performance of flax and pine fiber-reinforced polypropylene composites under UV aging, showcasing robust predictions for environmental durability (ANN for Mechanical Properties). Additionally, Bogrekci et al. (Ornaghi, Neves, and Monticeli 2021) utilized ANNs to predict compressive and tensile strengths of natural fiber-reinforced compressed earth blocks, demonstrating their versatility in optimizing construction materials (ANN for CEBs).

The research authored by M. Monticeli et al. (Monticeli, Neves, and Ornaghi Júnior 2021) explores the utilization of plant fibers as reinforcing in polymeric composites, highlighting their inherent features and potential applications. The thermal degradation behavior is of utmost importance in establishing the suitability for various temperature applications. Property prediction methods are currently popular in the field of materials research due to their ability to significantly decrease both cost and time. This study employs an ANN, methodology to forecast thermal deterioration curves. The network was trained using a heating rate of 10°C/min, 12 hidden layers, and an ideal training data set of 60. Additional computed heating rates demonstrated exceptional concurrence with empirical data. For any biomass source, R^2, the coefficient of determination, exceeds 0.99. The predictive fit and error sequence was as follows: *curaua* (1.8 %), *kenaf* (1.3 %), *ramie* (1.1 %), *jute* (1.9 %). Ultimately, RNAs may gain insight from their data and maximize processing, formulations, anticipate attributes and other combinations of incoming data. When compared to experimental data, predictive curves are very accurate. This means that mass loss can be forecast for different temperatures based on a set heating rate. The end result is that RNAs can learn from their data and improve the speed of processing, formulations, and the ability to guess traits based on different sets of input data. Predictive curves provide a high level of reliability when compared to experimental data. They allow for the prediction of mass loss at various temperatures based on the specified heating rate (Monticeli, Neves, and Ornaghi Júnior 2021).

Ornaghi et al. study the characteristics of lignocellulosic fibers used as reinforcement in polymer composites. Thermogravimetric Analysis (TGA) tests the thermal deterioration to find the highest

temperature at which these fibers can be used without losing a lot of mass. Equations based on the Arrhenius equation can be used to compute kinetic parameters by producing TG graphs at different heating rates. Nonetheless, it is helpful to have forecasting techniques for TG curves because every curve needs resources. TG curves for curaua fibers were produced in this study at four different heating rates: 5, 10, 20, and 40 °C/min. Then, the Vyazovkin kinetic parameters were determined using open-source software. An ANN was then trained to create curves for each heating rate between the lowest and highest rates used in the tests using the testing data. The newly projected curves at heating rates of 7, 15, 30, and 50 °C/min were used to confirm the kinetic parameters, yielding results that exactly matched the experimental ones. Ultimately, the integration of RNA and SRM offers a highly effective substitute for predicting TG curves that have not been verified experimentally, expanding the range of feasible uses (Ornaghi, Neves, and Monticeli 2021).

Focus point

The primary objective of this study is to enhance the prediction of thermal degradation behavior of *Dracaena draco* fibers by the utilization of artificial neural networks (ANNs). The major goal is to create a precise and effective artificial neural network (ANN) model that can use the kinetic characteristics of these fibers to predict their degradation at high temperatures. This paper is to evaluate the advantages, limits, and possibilities of the ANN model in enhancing the understanding and use of natural fiber composites by comparing it with conventional prediction methods.

Originality of the present study

The pioneering aspect of this study is in its investigation of Artificial Neural Networks (ANNs) as a means of forecasting the deterioration process of *Dracaena draco* fibers. Although artificial neural networks (ANNs) have been used in a range of applications in materials science, their use in the particular setting of natural fiber thermal deterioration remains largely uninvestigated. The present study makes a valuable contribution to the area by introducing a novel methodology for comprehending and forecasting the characteristics of these materials, hence potentially enhancing the effectiveness and sustainability of natural fiber composites.

Material and methods

Raw material

The mature *Dracaena draco* plants from the Algerian province of Algiers provided the *Dracaena draco* fibers (DDFs) employed in this investigation. With a height of over 20 meters at maturity, the Canary Island dragon tree resembles a gigantic parasol. It has a wide, flared base that holds up an extremely bushy, spherical crown that is 20 meters in circumference, supported by a thick network of interconnected branches. Because the plants were between 10 and 15 years old when they were harvested, the fiber maturity and content were consistent. In order to limit changes in chemical composition brought on by seasonal impacts and to coincide with ideal plant development conditions, the fibers were collected in May – June 2023, which is late spring to early summer. Prior to thermogravimetric analysis, the fibers from the collected leaves were manually extracted, washed, and dried for 48 hours at room temperature (25°C, 50% relative humidity) in sealed containers to avoid moisture absorption. Table 1 presents the morphological, thermophysical, physicochemical, and mechanical characteristics of DDFs.

Chemical analysis

Proximate and ultimate analysis techniques were used to assess the physicochemical characteristics of *Dracaena draco* fibers (DDFs) in order to clarify their chemical makeup and thermal behavior. Using a muffle furnace Carbolite Gero CWF 1100, the proximate analysis was carried out in compliance with the GB/T 212–2008 standard to ascertain the amounts of ash, volatile matter, and fixed carbon (Huang et al. 2017). About 1.0 ± 0.01 g of finely ground DDFs were put in ceramic crucibles and heated under controlled conditions. The fixed carbon and ash were then

Table 1. *Dracaena draco* fibers (DDFs) properties (Hadou, Belaadi, Alshahrani, et al. 2024) (Hadou, Belaadi, Alshaikh, et al. 2024).

Analysis	Properties	Values
Morphological characteristics	Average density (g/cm^3)	1.2043
	Linear density (Tex)	18.87
Thermophysical characteristics	Moisture recovery (%)	12.88
	Moisture content (%)	11.54
	Crystallite size (nm)	3.14
	Crystallinity index (%)	30.42
Tensil characteristics	Mean yield stress MPa)	553
	Strain at fracture (%)	2.5
	Young's modulus (GPa)	24.9
Ultimate analysis (wt.%) [a]	C	47.53
	H	6.34
	O	44.19
	N	1.62
	S	0.32
Proximate analysis (wt.%) [a]	Moisture [b]	11.79
	Ash	2.18
	Volatile fraction	77.28
	Fixed Carbon [b]	8.75
Compositional analysis (wt.%) [a]	Cellulose	45.43
	Hemicellulose	24.13
	Lignin	26.78
O to C ratio and H to C ratio [c]	O/C	0.69
	H/C	1.59
Molecular Formula	$CH_{1.59}\ O_{0.69}\ N_{0.029}\ S_{0.0025}$	-
Calorific Value (MJ/kg)	Higher heating value (HHV) [d]	19.95

measured by burning them for 30 minutes at 815°C in an oxygen atmosphere, and the volatile matter was measured by heating them for 6 minutes at 600°C in a nitrogen atmosphere. To guarantee reproducibility, the analysis was carried out three times, and the findings were presented as dry weight percentages. A CHNS/O elemental analyzer PerkinElmer 2400 Series II was used to measure the fibers' carbon (C), hydrogen (H), nitrogen (N), and oxygen (O) contents for the final analysis (Zanchet et al. 2019). A high-precision microbalance (Mettler Toledo XP6, ±0.001 mg) was used to weigh in tin capsules about 2–3 mg of pre-dried DDFs (dried in a vacuum oven at 60°C for 24 hours). The elemental components of the samples were converted into CO_2, H_2O, N_2, and CO (for O) by combustion at 975°C in an oxygen-rich environment. These components were then separated by gas chromatography and measured with a thermal conductivity detector (TCD). The analyzer was calibrated with acetanilide as a reference material, and measurements were conducted in triplicate to ensure accuracy. Oxygen content was calculated by difference (O% = 100% – (C% + H % + N% + ash%)). This integrated approach, combining proximate and ultimate analyses, provides a comprehensive characterization of DDFs by correlating their elemental composition with thermal properties, facilitating a deeper understanding of their degradation behavior (Ali et al. 2021).

DDFs thermogravimetric examination (TGA)

The *Dracaena draco* fibers were utilized as the materials for investigating the thermal degrading behavior.

A thorough dataset of Thermogravimetric Analysis (TGA) results was acquired using non-isothermal pyrolysis experiments. The experiments were carried out utilizing a Simultaneous Thermal Analyzer (TGA/DSC). Samples measuring between 11–17 mg were placed in a porcelain furnace and exposed to temperatures ranging from 25 to 800°C. The heating process was carried out using six different rates: 5, 10, 15, 20, 25, and 30°C/min. Prior to pyrolysis, the thermal analyzer underwent a 60-minute purging process to eliminate the presence of air. The test was conducted in an environment of nitrogen with a consistent flow rate of 100 ml/min.

The DTG curves were subjected to a smoothing procedure in order to minimize noise in the data. Precautions were taken to avoid adding any bias at the extreme ends of the observed divisions.

Process of thermal degradation

Pyrolysis is a process of thermal degradation that involves heating biological material and causing a variety of chemical reactions. Prior to the generation of volatile compounds, Burnham et al. noted that the process of cellulose heat degradation involves the formation of an intermediate reaction (Xiaowei 2015). Ornaghi Jr. et al. employed the F-test model-fitting technique to ascertain that the thermal breakdown of plant fibers entails both concurrent and parallel responses. The identification of each reaction is difficult since the fibers have different compositions. To accomplish this, one must employ pseudo-mechanistic models and possess prior knowledge of the chemical structure and pyrolysis behavior (Ornaghi et al. 2020). Orfao et al. conducted a study on the heat degradation of biomasses by examining three first-order independent processes. They found that their results aligned well with the existing literature (Huang et al. 2017). Hence, the pyrolysis process can be illustrated by the reaction scheme shown in Equation 1 (Conesa, Caballero, and Reyes-Labarta 2004).

$$F_{\text{pyrolysis}} \rightarrow (1-s)G + sS \tag{1}$$

where S is the solid residue, G is the gas produced, F represents the ratio of the specimen that undergoes decomposition, while sS denotes the yield coefficient of the solid fraction.

The kinetics of thermal degradation are analyzed by measuring the mass loss, which is the distinction among the initial sample (F) and the resulting residue (S) after decomposition. Equation 2 describes the global kinetics, which has been selected to follow nth-order kinetics.

$$\frac{dw}{dt} = \frac{dF}{dt} + \frac{dS}{dt} = -kF^n + ksF^n = -kF^n(1-s) \tag{2}$$

Equation 3 is provided if the rate constants exhibit an Arrhenius-type behavior, with adjustments to enhance fitting quality as described by Conesa et al. (Conesa, Caballero, and Reyes-Labarta 2004). The equation includes the variables k, k_{ref}, and k_0. The number k stands for the kinetic constant, k_{ref} for the pre-exponential factor at a certain temperature (T_{ref}), and k_0 for the pre-exponential constant.

$$\frac{dw}{dt} = -k_0F^n(1-s)\exp\left(-\frac{E_a}{RT}\right) = k_{ref}F^n(1-s)\exp\left[\frac{E_a}{R}\left(\frac{1}{T}-\frac{1}{T_{ref}}\right)\right] \tag{3}$$

The method of artificial neural networks (ANNs)

There are input, output, and hidden levels in a normal ANN. In each layer, the number of neurons is different. In this case, the input vectors are TG graphs at different heating rates that were found using Equation 3 and the suggested kinetic model. To copy the given values, the network changes the weighting of the connections between neurons. The study utilized a network consisting of 2 hidden layers. The temperature range spanned from 20 to 800 °C, with heating rates of 5, 10, 15, 20, 25, and 30 °C/min. The mass loss parameter was put in, and the weight reduction value was got out. The process plan is shown in Figure 1. The software utilized for this task was Origin Lab Pro 2024b, which employed the neural network technology as part of its programme.

It is important to set up the training process, figure out how many neurons are in the layer that is invisible, and check the quality of the first TG curves before using the networks. To avoid overtraining, it is best to keep the number of original TG curves used for training at a healthy level. By using different mixes of material, heating rate, and temperature in the ANN, three values are obtained that show small differences, which leads to good results. When you use these orthogonal combinations instead of random parameter choices, you get better results.

An ANN is a mathematical framework that is designed based on the functioning of the central nervous system in the brain. It has the ability to identify patterns and acquire the skill of making predictions through the use of empirical models. Neural networks have a diverse array of applications. To determine the optimal parameters for the prediction model, it is essential to perform tests on these models (Turco et al. 2021). The number of cells in the hidden layer is crucial in network architecture. The present investigation investigated various amounts of neurons in the hidden layer. The optimal amount changes depending on the specifics of

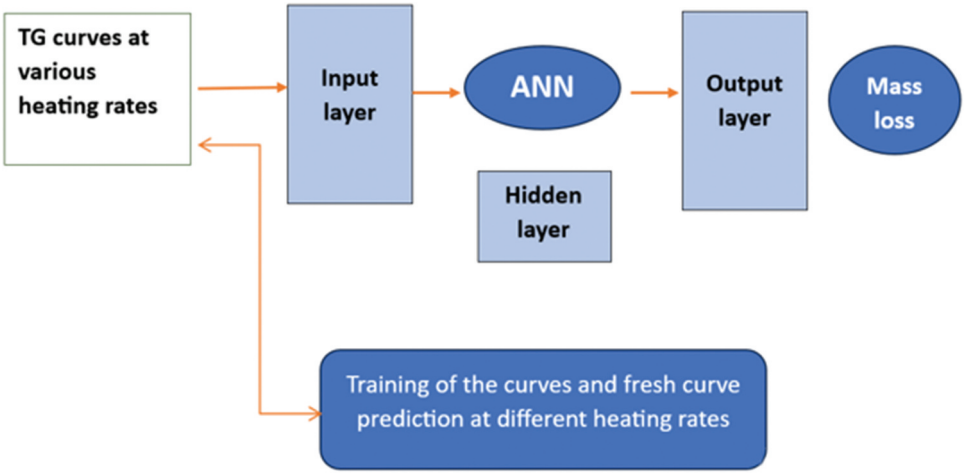

Figure 1. Schematic of an artificial neural network.

the issue in question and the training technique used, determined through a process of repeated experimentation (Altıntaş et al. 2019).

The appropriate number of hidden layers for our inquiry is determined by considering the regularization approach, early stopping generalization, curve analysis, kinetic information at different heating speeds, and thermogravimetric curves. The objective is to assess the regression's adequacy in fitting the target and actual parameter values. The transfer function employed in all ANNs is the hyperbolic tangent.

The artificial neural network was implemented based on the information provided in Figure 1. The prediction model was constructed utilizing the tan-sigmoidal transfer function, where A = tansig. In this context, the variable n denotes the quantity of testing data, while FP stands for alternative function variables. The activation function used in the concealed layers was defined as $f(x) = 1/(1 + e^{-x})$. The user's text is empty. To prevent constraining the output to a narrow range, the transfer function was implemented on both the concealed and output layers. The function examines the correlation among vegetable fiber, temperature, duration, and rate of heating in relation to the occurrence of mass reduction. The method of learning relies on the reverse propagation of an exponential search technique to train feedback artificial neural networks and supervise the process of learning. The optimality criterion of squared error among the predicted, desired, and measured values is assessed by the minimum sum. Additionally, the accurate computation of the gradient at each layer is achieved through the backward error flow, with separate consideration of the gradient computed for each layer (Altıntaş et al. 2019; Moayedi and Rezaei 2019).

The transfer function is a mathematical operation that transforms input signals into output signals. These signal outputs are subsequently employed to represent a functional curve of experimental data. The process of determining the ideal output with minimal error involves selecting the appropriate number of hidden layers and training iterations. Utilizing a reduced number of hidden layers will solely enable the representation of linear functions and result in faster computation. However, augmenting the number of layers can effectively represent an intricate curve fitting or arbitrary decision boundary, albeit at the expense of longer computational duration.

An ANN is a computer model that emulates the operation of the central nervous system in the brain. It has the ability to gather information from data and recognize patterns, allowing it to make predictions using empirical models. The utilization of neural networks has a wide range of potentialities. Nevertheless, it is crucial to conduct tests on these models in order to assess the most effective parameters for applying the prediction model (Conesa, Caballero, and Reyes-Labarta 2004). An essential factor to take into account in the network structure is the quantity of neurons present in the hidden layer. This study has examined various quantities of neurons in the subterranean layer. The ideal number of these neurons is contingent upon the training methodology employed and the particular conditions surrounding the event. The ideal number of neurons in each layer is found through a process of experimentation and refinement (Zhang and Friedrich 2003).

Equation 4 describes how the results of an experimental dataset, which was split into a training dataset and a projected dataset, were used to calculate the error. By employing the test dataset and evaluating its quality using the coefficient of determination (R^2), the efficacy of the procedure was determined. The error technique quantifies the degree to which the variability in the dependent variable (output) can be precisely forecasted based on the independent variable (input) using experimental degradation fit vs expected degradation fit. This concept has been deliberated about by (Pathak et al. 2020; Uzuner and Çekmecelioğlu 2016).

$$R^2 = 1 - \frac{\sum_{i=1}^{N} \left(H_i - H_{i,mol}\right)^2}{\sum_{i=1}^{N} \left(H_i - H_{i,avg}\right)^2} \tag{4}$$

The term "$H_{i,\ mol}$" reflects the output of the network. H_i refers to the target, while $H_{i,avg}$ represents the average of the target values.

To explain the link between the input and output variables, Equation 4 was applied. Predictive modeling techniques are used in this section to predict various input data combinations without the need for an experimental procedure. The goal is to reduce expenses and the duration of experiments while still ensuring statistical significance (Debnath, Reddy, and Yi 2016; Monticeli et al. 2020). To reduce inaccuracies, ANN predicted curves were used to create the 3D plane that represents the thermal degradation behavior for each curve. The error can be measured using the coefficient of determination, as defined in Equation 4, which quantifies the correlation between the experimental and projected fit.

$$Y = \beta_0 \sum_{i=1}^{k} \beta_0 H_i + \sum_{i=1}^{k} \beta_{ii} H_{ii}^2 + \sum_{j=1}^{k} \beta_0 H_j + \sum_{j=1}^{k} \beta_{jj} H_{jj}^2 + \sum_{i=1}^{k-1} \sum_{j=1}^{k} \beta_{ij} H_i H_j \tag{5}$$

Y depicts the projected curve, specifically the percentage of mass loss. i corresponds to the temperature variation T (°C) along the x-axis, while j corresponds to the heating rate (°C/min) along the y-axis. The constant term is represented by the symbol β_0, the linear coefficient by c_i, and the interaction coefficient by c_{ij}.

$$MAE = \frac{1}{N} \sum_{i=1}^{N} \left(H_i - H_{i,mol}\right) \tag{6}$$

$$MBE = \frac{\sum_{i=1}^{N} \left(H_i - H_{i,mol}\right)}{N} \tag{7}$$

$$RMSE = \sqrt{\frac{\sum_{i=1}^{N} \left(H_i - H_{i,mol}\right)^2}{N}} \tag{8}$$

Kinetic evaluation methods

The Flynn-Wall-Ozawa (FWO), Kissinger-Akahira-Sunose (KAS), and Starink (STR) methods were employed to compute the apparent activation energy using TGA data from experimental and optimal ANN predicted model data (Mishra et al. 2023). The rate of thermal breakdown, denoted as, can be computed using the Arrhenius equation:

$$\frac{d\alpha}{dT} = \frac{A}{\beta} \times \exp\left(-\frac{E_a}{RT}\right) f(\alpha) \tag{9}$$

The conversion rate (α), temperature (K), and heating rate (β) are measured in Kelvin per minute (K/min). The pre-exponential factor (A) is expressed in seconds to the power of a negative one (s^{-1}) and the ideal gas constant R is 0.008321 kJ/mol.K. The differential mechanism function (f(α)) depends on the specific value of α.

Computation of the degree of conversion (α) in TGA analysis can be achieved using Equation 9. The symbols M_0, M_f, and Mt represent the initial mass, final mass, and mass at a specific time (t) respectively (Kumar et al. 2021).

$$\alpha = \frac{M_0 - M_t}{M_0 - M_f} \tag{10}$$

The primary techniques employed for estimating kinetic parameters are model-fitting and isoconversional model-free (Fu et al. 2023). This work establishes the activation energy and pre-exponential factor of experimental and best predicted model data using artificial neural networks for the initial phase of thermal degradation of solid-state reactors (DDFs) utilizing three commonly used model-free approaches.

Kissinger-Akahira-Sunose (KAS) method

An extension of the Coats-Redfern method is the Kissinger-Akahira-Sunose (KAS) strategy, which can be defined as follows (W. Zhang et al. 2021):

$$\ln\left(\frac{\beta}{T^2}\right) = -\frac{E_a}{RT} + ln\left(\frac{AE_a}{Rg(\alpha)}\right) \tag{11}$$

In order to determine the activation energy for the KAS approach, one can compute the gradient of the lines generated when ln(β/T2) is graphed versus 1/T.

Flynn-Wall-Ozawa (FWO) method

The equation obtained from Doyle's computational analysis of the Flynn-Wall-Ozawa (FWO) method is stated as (Kozlov et al. 2017):

$$\ln(\beta) = -1.052\frac{E_a}{RT} + ln\left(\frac{AE_a}{Rg(\alpha)}\right) - 5.331 \tag{12}$$

Utilizing the FWO method, the activation energy is determined by analyzing the linearized plot of ln (β) vs. (1/T). This method yields an activation energy, denoted as Ea, that is equivalent to (-Ea/R), which corresponds to the slope of the resulting line.

Starink (STR) method

The Starink model is regarded as a non-isothermal model-free method of analysis (M. Kumar et al. 2021).

$$\ln\left(\frac{\beta}{T^{1.92}}\right) = C - 1.0008\frac{E_a}{RT} \tag{13}$$

The activation energy for the STR approach is determined by examining the gradient of the lines generated when the natural logarithm of β/T1.92 is graphed versus 1/T.

The pre-exponential component (A) is obtained using the Kissinger technique and can be expressed as follows (Ding et al. 2022):

$$A = \frac{\beta E_a e^{\left(\frac{E_a}{RT_m}\right)}}{RT_m^2} \tag{14}$$

The maximum temperature appearing on the DTG curve is represented by Tm (K).

Thermodynamics analysis

Through utilizing the values of A, it is possible to compute and compare the thermodynamic characteristics of the experimental results with the data predicted by the ideal artificial neural network (ANN). These characteristics include the enthalpy change (ΔH), the Gibbs free energy change (ΔG), and the entropy change (ΔS). One approach to convey these characteristics is as follows (M. Kumar et al. 2021; Tabal et al. 2021; Wang et al. 2023):

$$\Delta H = E_a - RT_m \tag{15}$$

$$\Delta G = E_a + RT_m \ln\left(\frac{K_B T_m}{hA}\right) \tag{16}$$

$$\Delta S = \frac{\Delta H - \Delta G}{T_m} \tag{17}$$

The Planck constant (h) is defined as 6.626×10^{-34} J/s, and the Boltzmann constant (KB) is defined as 1.381×10^{-23} J/K.

Results and discussion

Chemical analysis

DDFs constitute a promising biomass for thermal conversion due to their beneficial attributes: low moisture content (11.79%), high volatile matter content (77.28%), minimal ash content (2.18%), considerable fixed carbon content (8.75%), advantageous elemental composition, elevated hydrogen-to-carbon ratio (H/C = 1.59), low oxygen-to-carbon ratio (O/C = 0.69), high calorific value (19.95 MJ/kg), and substantial lignin content (26.78%), as detailed in Table 1. The attributes of DDFs make them highly appropriate for pyrolysis, gasification, and combustion processes (Hadou, Belaadi, Alshahrani, et al. 2024; Hadou, Belaadi, Alshaikh, et al. 2024).

Features of thermal degradation

Figure 2 presents the thermogravimetric (TG) curves of *Dracaena draco* fibers at heating rates of 5, 10, 15, 20, 25, and 30 °C/min. The curve behavior is influenced by the biomass's chemical composition, as shown in studies (Hadou, Belaadi, Alshahrani, et al. 2024; Hadou, Belaadi, Alshaikh, et al. 2024). Thermal degradation of lignocellulosic materials involves three main stages: hemicellulose, cellulose, and lignin degradation. Unrelated to thermal degradation, a mass loss at about 100°C is caused by humidity release and the vaporization of extractables, waxy substance, and low-molecular-weight compounds.

Increased hemicellulose content correlates with higher moisture absorption, contributing to the thermal stability of the fibers (Aquino et al. 2007; Motta Neves et al. 2020; Poletto, Ornaghi Junior, and Zattera 2014). All fibers displayed similar thermal stability. Cellulose is responsible for significant mass loss at around 250°C (Sunphorka, Chalermsinsuwan, and Piumsomboon 2017). It is possible that the main lignin degradation occurs at around 400°. Interestingly, a higher lignin concentration does not always result in increased residue content due to varying degradation patterns at different temperatures. Table 2 delineates the specifics of the sample's devolatilization in relation to the heating rate.

Lignin degrades over a wide temperature range, so more lignin in fibers means more components breaking down at both higher and lower temperatures. Generally, TG curves for plant fibers exhibit consistent patterns regardless of chemical composition (John and Thomas 2008; Sánchez-Jiménez et al. 2009; Yao et al. 2008). Predicting mass loss using artificial neural network (ANN) models is more challenging for fibers like *curaua* and *jute* compared to kenaf and ramie. According to Chen et al., higher

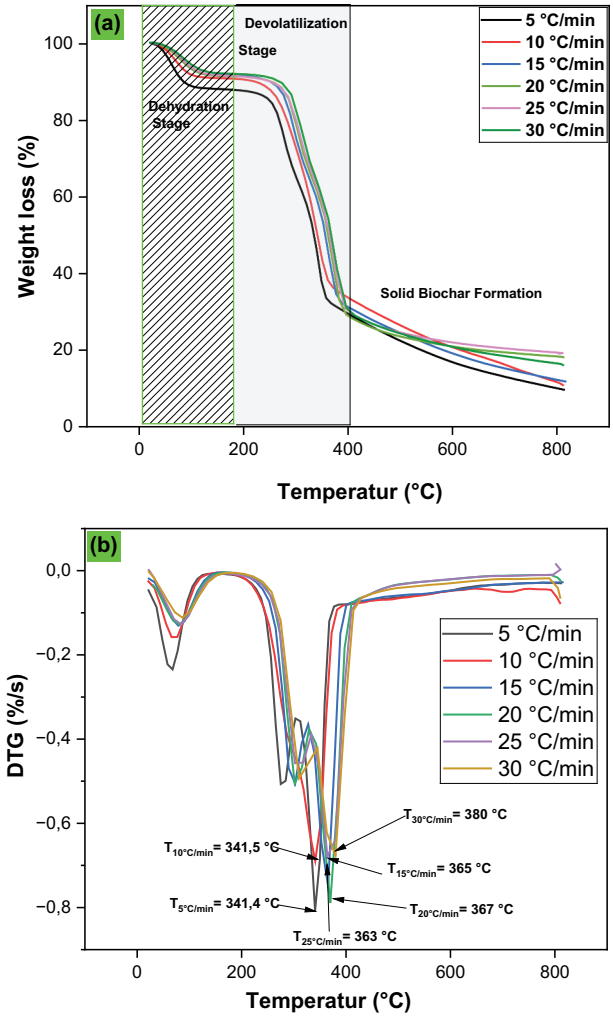

Figure 2. (a) TGA, and (b) DTG profiles of DDFs at different heating rates.

Table 2. TGA/DTG parameters of DDFs at different heating rates.

	First devolatilization zone/°C		Second devolatilization zone/°C				
Heating rate min/°C	DTG	TGA	DTG	TGA	T5 (°C)	T10 (°C)	T50 (°C)
5	233–278	233–302	306–340	319–356	230	250	320
10	232–286	238–286	311–339	311–358	235	255	325
15	228–300	257–304	317–404	325–377	240	260	330
20	253–315	234–318	331–416	335–394	245	265	335
25	255–317	256–339	333–428	347–395	250	270	340
30	260–324	277–349	341–431	350–397	255	275	345

hemicellulose and cellulose concentrations cause more fluctuation in mass loss, complicating accurate predictions (D. Chen et al. 2018).

Key stages of thermal degradation are depicted in the table above, which shows the T5, T10, and T50% values obtained from the thermogravimetric (TG) curves of *Dracaena draco* fibers (DDFs) at heating rates of 5, 10, 15, 20, 25, and 30°C/min. With a temperature range of 230°C at 5°C/min to 255°C at 30°C/min, T5, or 5% mass loss, indicates the beginning of degradation, mostly as a result of moisture release and volatile decomposition. At 10% mass loss, T10 rises from 250°C to 275°C at the same heating rates, indicating more early degradation development. T50%, which denotes 50% mass loss, changes from 320°C to 345°C, indicating the primary phase of decomposition that involves the breakdown of cellulose and hemicellulose. A thermal lag effect, in which quicker heating postpones degradation events because there is less time for mass loss at lower temperatures, is demonstrated by these steady temperature increases with greater heating

rates. This behavior highlights how heating dynamics affect DDFs' thermal stability and offers important information for maximizing their use in procedures like pyrolysis or composite fabrication that call for thermal resistance.

ANN model for TGA and DTG

Table 3 and Table 4 displays the training efficacy outcomes of an Artificial Neural Network (ANN) with different network configurations, such as varied numbers of hidden layers and neurons. The most optimal model, ANN27, consists of two concealed layers: the initial layer comprises five neurons, while the next layer comprises 17 neurons. The ANN architecture with dimensions $5 \times 17 * 1$ was selected based on its low Mean Absolute Error (MAE) of 0.2204, Mean Bias Error (MBE) of −0.0287, Root Mean Square Error (RMSE) of 0.4993, and a high R^2 value of 0.99966. The ANN model was used to predict the thermal degradation features of DDFs, as shown in Figure 3. The variance between anticipated TG/DTG and target TGA/DTTG at various heating rates is shown in Figure 5. In addition, the Estimation of Ea (kJ/mol) and a (s −1) values for experimental and optimal ANN-predicted model data presented in Table 5.

A total of 220 iterations were executed, and the highest validation performance (0.056883) was achieved at the 33rd epoch, as depicted in Figure 4. The variance between anticipated TG/DTG and target TGA/DTTG at various heating rates is shown in Figure 5. The ANN models accurately predict the pyrolysis domains, curve shapes, and pseudo-component sizes, closely matching the experimental data's partial degradation curves (Jiang et al. 2022; Wang et al. 2024)

Figure 6 displays the ANN regression plot for each heating rate, showing negligible deviations across all speeds. The linear relationship between the anticipated output and experimental data confirms a strong match, with a coefficient of determination of 0.99. This linearity in different materials suggests that plant fibers exhibit similar reliability. The agreement between experimental and projected mass loss responses further supports the ANN model's reproducibility for studying plant fiber thermal degradation.

The accuracy of transfer functions is greater for test data than for training data. A 20-box error histogram (Figure 7) shows error analysis, with the test and training data sets exhibiting relatively low occurrences of significant errors. Significantly, the number of errors in the test is lower than the number of errors in the training, which aligns with the accuracy findings shown in Figure 6.

Figure 8 presents the residuals graph for each heating rate. The likelihood residual graph has a linear scatter pattern that aligns with the extrapolation trend line, suggesting that the residuals adhere to a normal distribution. The residuals for heating rates of 5 and 10°C/min exhibit a random and uniform distribution around the horizontal line, suggesting a robust fit of the model. When the temperature increases at a pace of 15°C/min, there is evidence of heteroscedasticity, which is characterized by an increase in residual variability. At 20°C/min, extreme residuals suggest model fitting issues or outliers. At 25°C/min, a consistent decrease in residuals suggests a tendency to overestimate at higher temperatures. Finally, at 30°C/min, residuals are evenly spread, with a greater spread at lower temperatures, indicating room for model improvement.

In summary, the model performs well at slower heating rates (5 and 10°C/min) but requires modifications at higher rates (15 to 30°C/min) to address heteroscedasticity and systematic bias.

The application of ANN was appropriately executed, utilizing a consistent methodology across heating rates of 5–30 °C/min. This approach facilitated the creation of a deterioration curve, predicted by the ANN, for heating rates that could not be empirically measured. Figure 9 illustrates a three-dimensional plane where the Z axis denotes mass loss, The X-axis represents temperature, while the Y-axis represents heating rate. Specific plant fibers are depicted as black dots on the experimental degradation curve. This methodology allows for reliable prediction of the deterioration curve's characteristics at various heating rates and temperatures, reducing the number of tests and associated costs. Moreover, it assists in ascertaining the dissociation energy of enduring bonds for each strengthening element and associated results.

As the heating rate increases, the starting temperature at which degradation occurs generally increases, but the amount of residue left behind reduces for all curves. The graphs show the varied degradation behaviors of lignin, cellulose, and hemicellulose with different heating rates, influenced by their composition and degradation mechanisms (W.-H. Chen et al. 2019; Ornaghi et al. 2014; Yeo et al. 2019). The DDF degradation curves exhibit a consistent rise during both the initial and ultimate stages of degradation.

Table 3. RMSE and R^2 of different ANN network structure for DDFs.

			β = 5°C/min		β = 10°C/min		β = 15°C/min		β = 20°C/min		β = 25°C/min		β = 30°C/min	
Model	Inputs	Network topology	RMSE	R^2	RMSE	R^2	RMSE	R^2	RMSE	R^2	RMSE	R^2	RMSE	R^2
ANN 1	Temperature	3 × 1	1.631	0.99882	1.992	0.99841	2.7244	0.99888	2.8079	0.99895	2.4677	0.99887	2.0976	0.99887
ANN 2	Heating rate	5 × 1	1.8744	0.9986	2.3597	0.998	2.0755	0.99847	2.2377	0.99854	2.358	0.99846	2.2786	0.99846
ANN 3		7 × 1	1.7119	0.99875	1.291	0.99898	1.3188	0.99945	1.5252	0.99952	1.6624	0.99944	1.728	0.99944
ANN 4		9 × 1	1.5701	0.99887	1.7286	0.99866	1.8577	0.99913	2.2886	0.9992	2.4564	0.99912	2.4711	0.99912
ANN 5		11 × 1	1.3935	0.999	1.2957	0.99898	1.2529	0.99945	1.1067	0.99952	1.1984	0.99944	1.2044	0.99944
ANN 6		13 × 1	1.1916	0.99913	1.0865	0.99909	1.7212	0.99956	1.7068	0.99963	1.5818	0.99955	1.4841	0.99955
ANN 7		15 × 1	1.2283	0.99911	1.1611	0.99906	1.2058	0.99953	1.145	0.9996	1.2899	0.99952	1.3306	0.99952
ANN 8		17 × 1	1.0582	0.9992	0.9649	0.99915	1.0585	0.99962	0.9394	0.99969	1.0077	0.99961	1.0401	0.99961
ANN 9		19 × 1	0.5518	0.99937	0.5208	0.99928	0.6399	0.99975	0.5632	0.99982	0.5714	0.99974	0.6366	0.99974
ANN 10		3 × 3 * 1	1.4083	0.99899	2.01	0.99839	2.5803	0.99886	2.6017	0.99893	2.5136	0.99885	2.1717	0.99885
ANN 11		3 × 5 * 1	1.4304	0.99898	2.0555	0.99834	2.3107	0.99881	2.4994	0.99888	1.4245	0.9988	1.4646	0.9988
ANN 12		3 × 7 * 1	1.6651	0.99879	1.691	0.99869	1.6431	0.99916	1.7673	0.99923	1.6978	0.99915	1.7858	0.99915
ANN 13		3 × 9 * 1	1.7091	0.99875	1.8188	0.99858	1.2187	0.99905	1.4765	0.99912	1.3622	0.99904	1.4694	0.99904
ANN 14		3 × 11 * 1	1.2177	0.99912	1.13	0.99907	1.1047	0.99954	0.883	0.99961	0.9853	0.99953	1.0795	0.99953
ANN 15		3 × 13 * 1	1.2515	0.9991	1.1408	0.99907	1.5554	0.99954	1.6806	0.99961	1.4676	0.99953	1.3182	0.99953
ANN 16		3 × 15 * 1	1.1086	0.99918	1.0982	0.99909	1.045	0.99956	0.9972	0.99963	1.5322	0.99955	1.3086	0.99955
ANN 17		3 × 17 * 1	1.2035	0.99912	1.1736	0.99905	1.9814	0.99952	2.8706	0.99959	1.6114	0.99951	2.0884	0.99951
ANN 18		3 × 19 * 1	1.3465	0.99903	1.2474	0.99901	1.266	0.99948	1.0095	0.99955	1.1991	0.99947	1.3063	0.99947
ANN 19		5 × 3 * 1	1.4083	0.99899	1.853	0.99855	1.1082	0.99902	1.245	0.99909	0.8568	0.99901	0.8032	0.99901
ANN 20		5 × 5 * 1	1.918	0.99856	1.6682	0.99871	1.5863	0.99918	1.1829	0.99925	1.6859	0.99917	1.721	0.99917
ANN 21		5 × 7 * 1	0.7573	0.99922	1.003	0.99913	1.227	0.9996	1.7649	0.99967	1.4417	0.99959	1.6901	0.99959
ANN 22		5 × 9 * 1	1.5306	0.9989	2.0977	0.9983	1.5503	0.99877	1.6372	0.99884	1.3603	0.99876	2.0488	0.99876
ANN 23		5 × 11 * 1	0.5743	0.99937	0.625	0.99926	0.4831	0.99973	0.6091	0.9998	0.5365	0.99972	0.594	0.99972
ANN 24		5 × 13 * 1	1.1692	0.99914	1.052	0.99911	1.2246	0.99958	1.4361	0.99965	1.318	0.99957	1.3208	0.99957
ANN 25		5 × 15 * 1	1.2836	0.99908	1.1626	0.99905	1.2018	0.99952	0.9577	0.99959	1.0379	0.99951	1.14	0.99951
ANN 26		5 × 17 * 1	0.4568	0.99939	0.5255	0.99928	0.5467	0.99975	0.658	0.99982	0.4298	0.99974	0.4735	0.99974
ANN 27		5 × 19 * 1	1.5395	0.9989	1.6544	0.99872	1.5474	0.99919	1.3986	0.99926	1.3978	0.99918	1.457	0.99918

Table 4. The MBE and MAE of different ANN network structure for DDFs.

			β = 5°C/min		β = 10°C/min		β = 15°C/min		β = 20°C/min		β = 25°C/min		β = 30°C/min	
Model	Inputs	Network topology	MBE	MAE	MBE	MAE	MBE	MAE	MBE	MAE	MBE	MAE	MBE	MAE
ANN 1	Temperature	3 × 1	−0.0406	1.4457	0.9083	0.7467	−1.7603	2.5972	0.1093	2.5606	0.8795	2.137	−0.6092	1.8565
ANN 2	Heating rate	5 × 1	−0.4607	1.5642	1.4069	0.672	−0.6175	1.9366	−0.4113	1.9476	0.2327	2.0878	−0.19	1.8777
ANN 3		7 × 1	−0.1704	1.3067	0.2226	0.7162	−0.0844	1.132	0.0978	1.4119	0.0224	1.5363	−0.0856	1.4794
ANN 4		9 × 1	−0.12	1.3421	0.2179	0.5573	−0.3032	1.6503	0.1786	2.0474	1.2779	2.1332	−0.5894	2.115
ANN 5		11 × 1	−0.0936	1.068	0.0309	0.5936	−0.0576	1.0331	0.1177	1.0202	0.061	1.0048	0.1146	0.9128
ANN 6		13 × 1	0.0845	0.9496	−0.0272	0.5528	−0.1047	1.375	−0.1257	1.4835	0.4421	1.1946	−0.456	1.1128
ANN 7		15 × 1	−0.05	0.9037	−0.0924	0.5353	0.0847	0.9894	−0.1062	0.986	0.0479	1.0744	−0.1857	1.0561
ANN 8		17 × 1	−0.0514	0.8509	0.0458	0.5353	−0.0255	0.9392	0.0583	0.8557	0.1034	0.8532	−0.0065	0.8661
ANN 9		19 × 1	−0.0514	0.5618	0.0458	0.6317	−0.0255	0.6332	0.0583	0.5994	0.1034	0.6263	−0.0065	0.6897
ANN 10		3 × 3 * 1	−0.1263	1.0696	0.8848	0.7053	−1.7401	2.4851	0.1602	2.3578	0.9935	2.1582	−0.3092	1.9502
ANN 11		3 × 5 * 1	0.1337	1.1481	1.1452	0.7296	−1.4847	2.0707	0.2947	2.0818	0.1359	1.207	0.0227	1.2838
ANN 12		3 × 7 * 1	−0.26	1.4281	−0.306	0.4683	−0.1585	1.3029	0.0014	1.5208	−0.044	1.4358	−0.1115	1.5355
ANN 13		3 × 9 * 1	−0.7038	1.4639	0.76	0.3293	−0.3884	1.1882	0.4814	1.1924	−0.1686	1.088	−0.2117	1.0847
ANN 14		3 × 11 * 1	−0.0207	1.0043	−0.0605	0.2965	−0.0424	0.954	0.0617	0.765	0.1493	0.9109	−0.1726	0.9139
ANN 15		3 × 13 * 1	0.1094	0.9601	−0.039	0.277	−0.4083	1.051	0.5437	1.2523	−0.1162	1.2789	0.2808	1.1156
ANN 16		3 × 15 * 1	−0.0738	0.8962	0.0992	0.7385	−0.0966	0.8667	−0.0986	0.919	0.2274	1.2161	−0.0677	1.1459
ANN 17		3 × 17 * 1	0.176	0.9013	0.1836	0.2204	−0.014	1.5261	0.7593	2.2662	0.4876	1.3146	−0.8614	1.627
ANN 18		3 × 19 * 1	0.176	1.0687	0.1836	0.2831	−0.014	0.901	0.7593	0.8477	0.4876	0.8946	−0.8614	1.1067
ANN 19		5 × 3 * 1	−0.1263	1.0696	1.095	0.4743	−0.6071	1.101	0.3296	1.0335	−0.314	0.875	0.2712	0.8431
ANN 20		5 × 5 * 1	−0.0461	1.576	0.4182	0.437	0.0822	1.2071	0.1042	0.993	0.2765	1.2013	−0.2217	1.2739
ANN 21		5 × 7 * 1	0.1048	0.7034	0.0705	0.2284	−0.0171	1.0012	0.1873	1.4591	0.0989	1.1988	−0.4881	1.3757
ANN 22		5 × 9 * 1	−0.645	1.3636	1.3387	0.5241	−0.773	1.3561	−0.0294	1.4455	0.0599	1.11	−0.5	1.3769
ANN 23		5 × 11 * 1	0.0246	0.5321	−0.0189	0.0749	0.0119	0.5386	0.0454	0.6249	−0.0062	0.5793	−0.0596	0.5709
ANN 24		5 × 13 * 1	0.0924	0.8041	−0.0609	0.3576	−0.0641	0.9013	0.2967	1.1762	−0.1924	1.0432	−0.1775	1.0063
ANN 25		5 × 15 * 1	−0.1374	1.0045	0.0524	0.4673	0.0066	0.9297	−0.0276	0.8148	0.0985	0.902	−0.0598	0.916
ANN 26		5 × 17 * 1	0.0213	0.4981	0.0208	0.3017	−0.0117	0.5351	−0.0031	0.5963	0.0396	0.515	0.0142	0.5263
ANN 27		5 × 19 * 1	0.0213	1.2129	0.0208	0.2507	−0.0117	1.3241	−0.0031	1.2479	0.0396	1.0617	0.0142	1.099

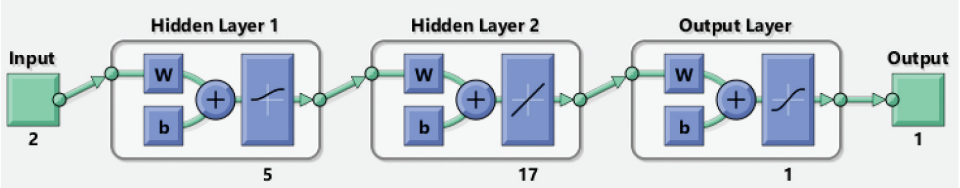

Figure 3. The network topology represents the most optimal structure for predicting DDFs using an ANN.

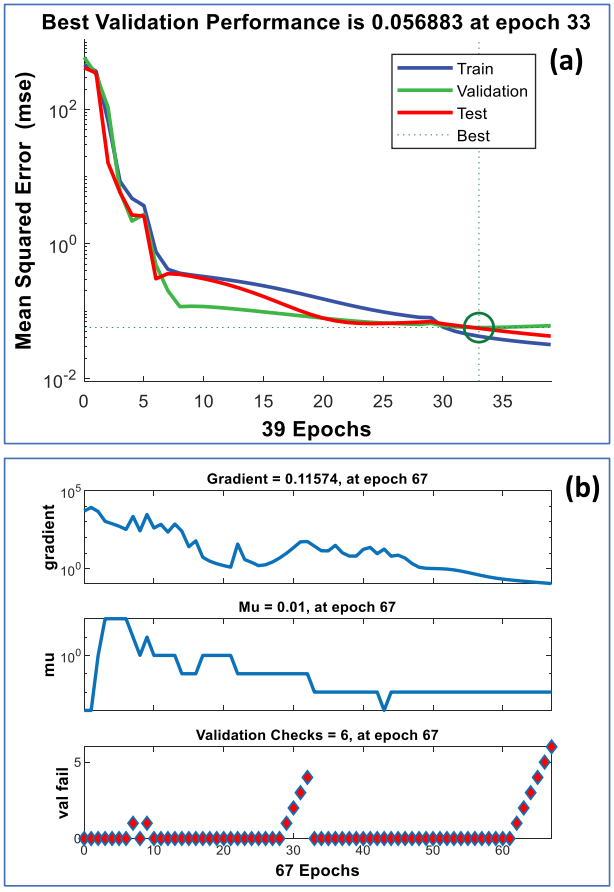

Figure 4. The optimal model projected by the ANN for both the validation and training datasets.

Moukhina analyzes the thermogravimetric behavior curves and investigates the correlation between activation energy and the level of conversion for the heating rate of a multi-step process (Moukhina 2012). These reactions encompass sequential, competitive, and independent processes. Moukhina's work indicates that the TG curves observed here imply a series of reactions occurring in a specific order. Ornaghi Ju'nior et al. discovered in a prior study that the activation energy is directly correlated with the extent of conversion. This relationship is atypical for a consecutive reaction. The observed difference indicates that the deterioration of plant fibers due to heat involves a mixture of reaction pathways, including sequential, parallel, independent, and overlapping responses (Ornaghi et al. 2020).

Kinetic analysis methods

The activation energy (Ea) and pre-exponential factor (A) were estimated using three model-free kinetic methods (FWO, KAS, and STR), as shown in. The parameter α increased incrementally from 0.10 to 0.90 at uniform intervals of 0.10, as illustrated in Figure 10. The experimental activation energy (Ea) values, obtained by the KAS method, range from 108.250 to 152.774 kJ/mol, with an average of 131.244 kJ/mol.

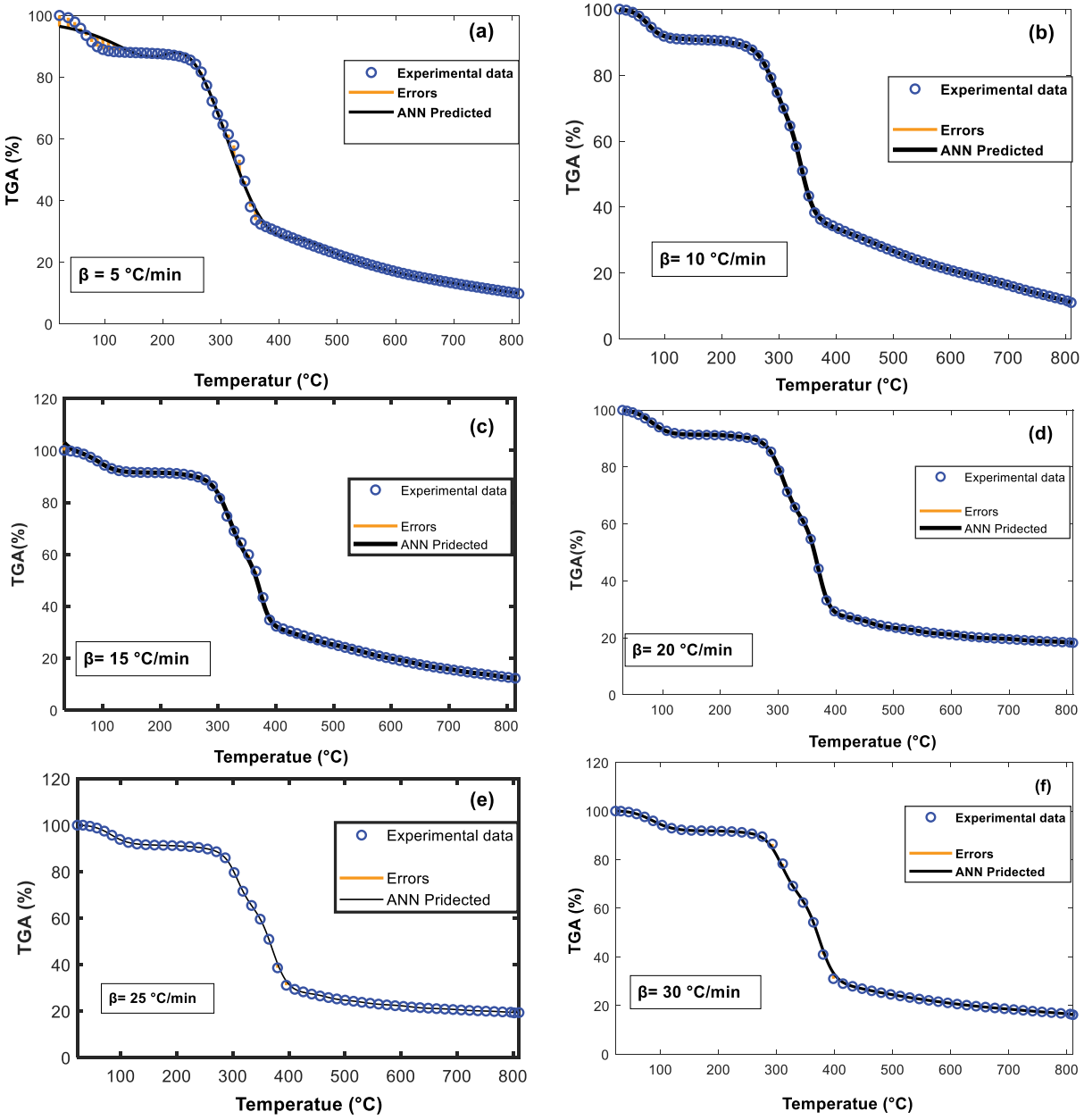

Figure 5. Comparison of the mass loss at heating rates of 5, 10, 15, 20, 25, and 30 °C/min between the observed and projected values.

On the other hand, the Ea values estimated by ANN27 are systematically greater, varying from 107.945 to 157.585 kJ/mol, with an average of 133.420 kJ/mol. Furthermore, the values of the pre-exponential factor (A) demonstrate a comparable inclination. The mean experimental values are 3.53×10^{12} s^{-1}, however the average projected values using ANN27 are significantly higher, averaging 7.92×10^{25} s^{-1}. Consequently, the ANN27 model forecasts a higher energy barrier for the pyrolysis process, indicating a greater energy input for material degradation than what has been empirically seen. This overestimation may suggest that the artificial neural network (ANN) model is more prudent in its predictions or is more responsive to specific variables affecting the breakdown kinetics (V. K. Kumar, Hallad, and Panwar 2024).

The FWO approach exhibits a comparable pattern, as evidenced by experimental Ea values ranging from 104.010 to 113.877 kJ/mol, with an average of 109.269 kJ/mol. The projected Ea values estimated by ANN27 are once again elevated, ranging from 42.790 to 67.362 kJ/mol, with an average of 53.692 kJ. Compared to the observed A values, which average 7.85×1014 s^{-1}, the average predicted by ANN27 is somewhat lower, at 1.45×10^{10} s^{-1}. While the trend in Ea values does not differ much from that observed with the KAS

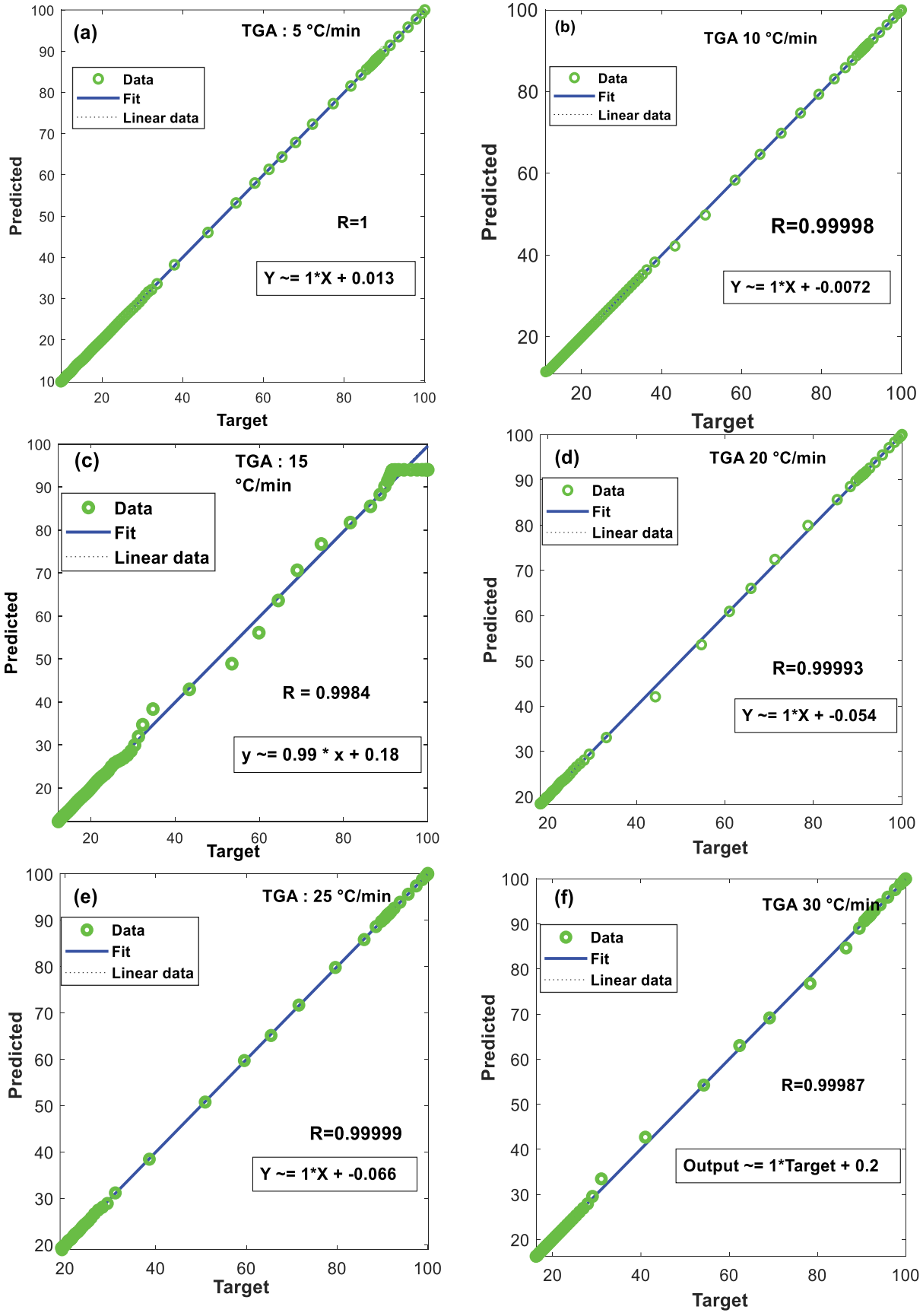

Figure 6. Plotting the parity between the goal and projected values.

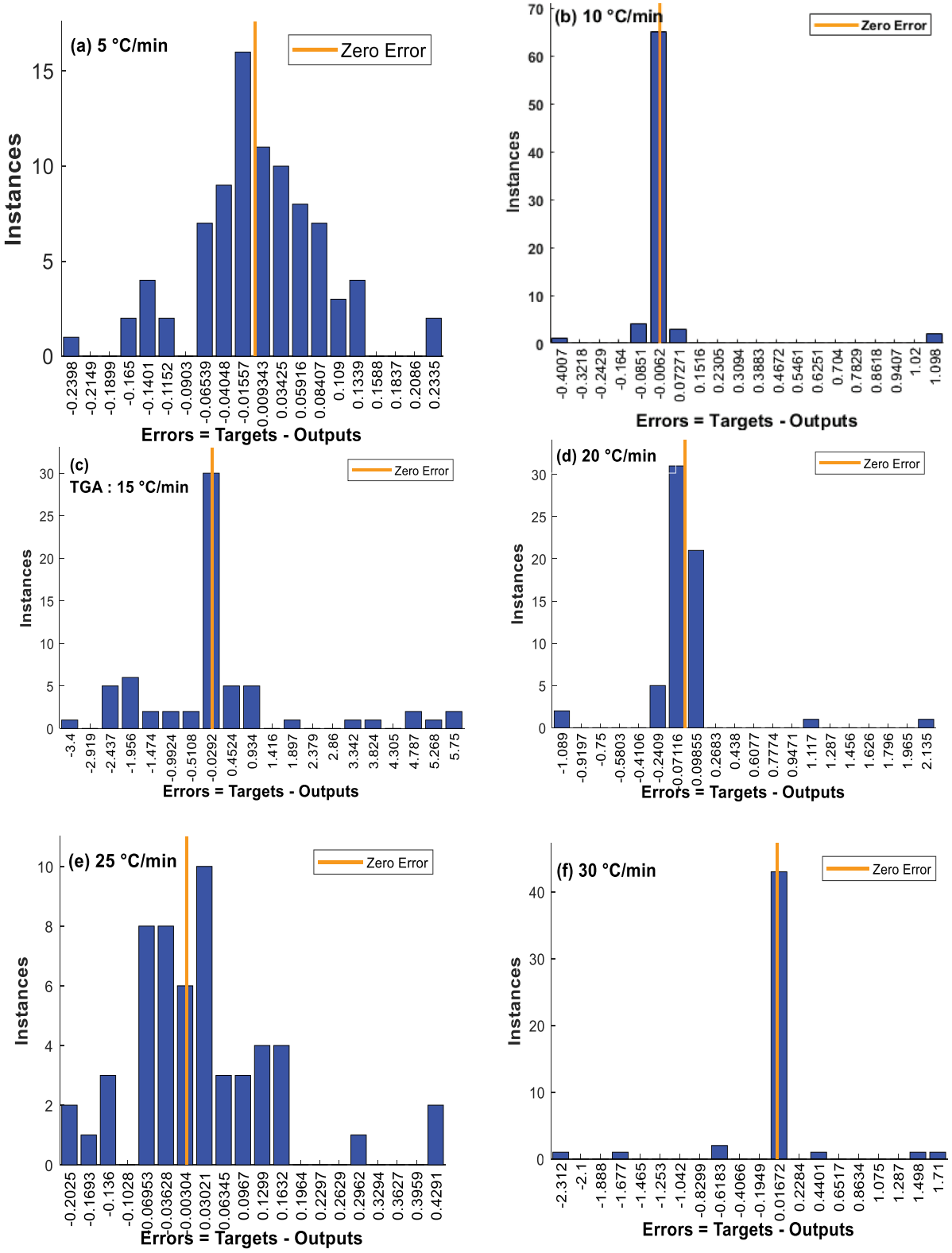

Figure 7. Error histogram plots with 20 bins.

technique, the reduced variations in pre-exponential factor values suggest that the ANN model may provide more precise predictions of the frequency of successful molecular collisions in the FWO approach. Nevertheless, the expected higher Ea values of the ANN27 model still indicate a tendency to overestimate (Padma et al. 2024).

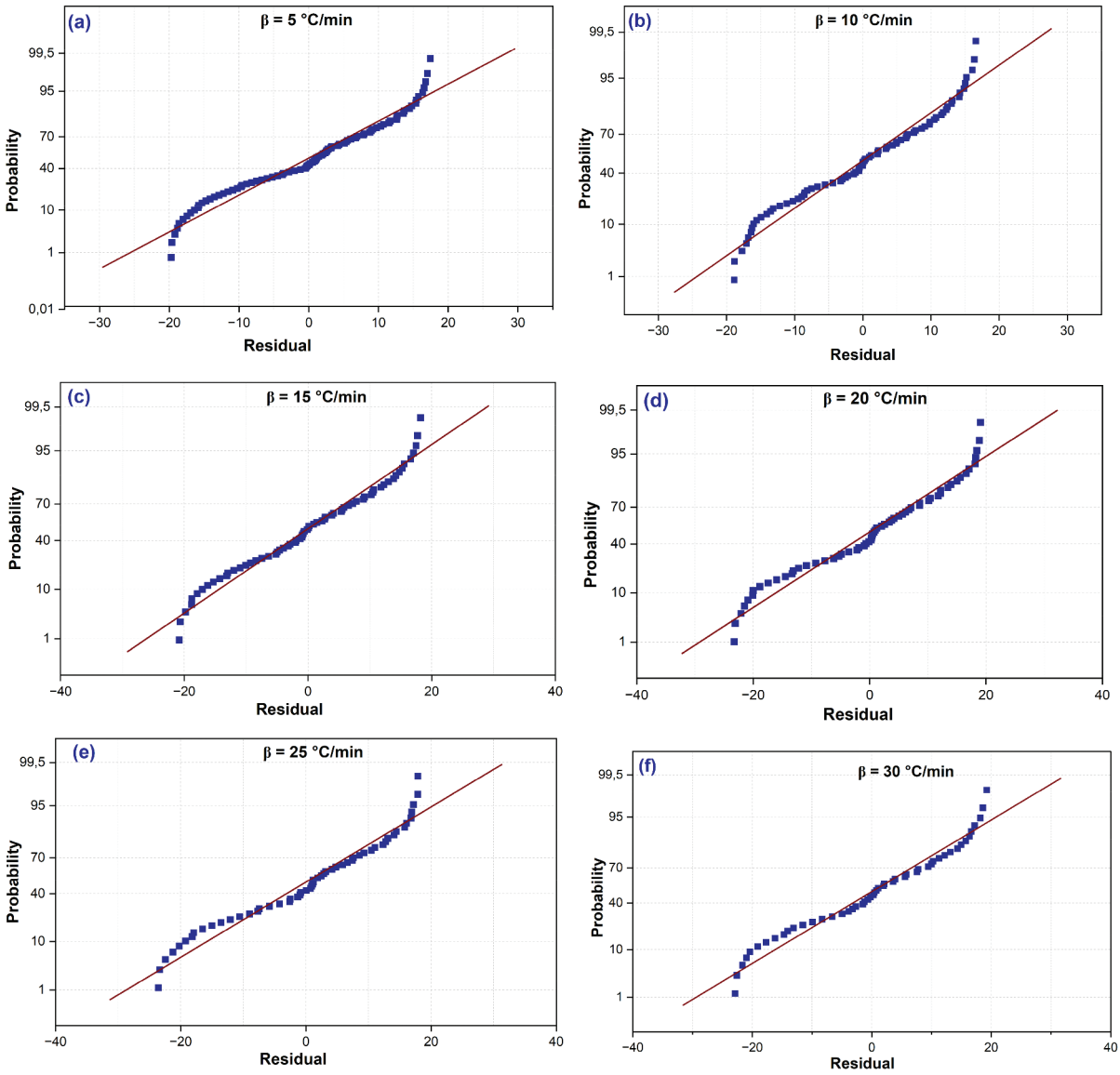

Figure 8. ANN residual plot.

The STR strategy yields the most extensive spectrum of Ea values among the three techniques. The measured energy absorption (Ea) values range from 108.604 to 153.358 kJ/mol, with an average of 131.694 kJ/mol. By contrast, the anticipated values of ANN27 range from 140.49 to 185.19 kJ/mol, with an average density of 177.47 kJ/mol. The experimental mean of 6.78×10^{11} s^{-1} dramatically falls short of the expected mean of 1.43×10^{12} s^{-1} obtained by ANN27. The substantial discrepancy in pre-exponential factor values between experimental and ANN27-predicted data suggests that the ANN model may not sufficiently capture the complexities of reaction kinetics when using the STR method. This discrepancy indicates that the ANN27 model may require more refinement to more accurately correspond to the experimental data, especially in the prediction of the pre-exponential component (Padma et al. 2024). Optimal artificial neural network (ANN) model predictions routinely estimate the activation energy (Ea) higher than experimental data in two out of the three motor modalities. Although this demonstrates that the forecasts of the ANN model may be cautious, it also prompts inquiries over its precision, particularly in real-world scenarios where exact energy needs are highly important. The levels of concurrence among the pre-exponential components (A) differ between the empirical data and the data predicted by the artificial neural network (ANN). The significant variations in the values of the pre-exponential

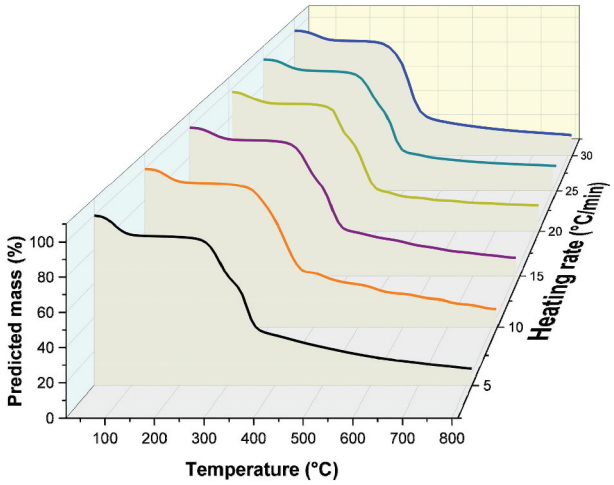

Figure 9. The ANN model utilizes a 3-dimensional prediction plane to estimate thermal degradation based on temperature and heating rate.

Table 5. Estimation of E_a (kJ/mol) and a (s^{-1}) values using three model-free methods for experimental and optimal ANN-predicted model data.

		Experimental data		Optimal ANN-predicted data	
Methods	α	Ea (kJ/mol)	A (s^{-1})	Ea (kJ/mol)	A (s^{-1})
KAS	**0.1**	108.250	4.23×10^{9}	107.945	3.88×10^{9}
	0.2	110.640	4.47×10^{9}	110.924	4.60×10^{9}
	0.3	114.020	5.57×10^{9}	113.705	5.04×10^{9}
	0.4	121.769	1.56×10^{10}	121.712	1.50×10^{10}
	0.5	134.555	1.26×10^{11}	137.082	2.04×10^{11}
	0.6	144.563	6.38×10^{11}	148.328	1.31×10^{20}
	0.7	146.850	7.14×10^{11}	151.012	1.56×10^{20}
	0.8	147.774	6.05×10^{10}	152.483	1.46×10^{19}
	0.9	152.774	1.06×10^{12}	157.585	2.56×10^{26}
	Avg	131.244	3.53×10^{12}	133.420	7.92×10^{25}
FWO	**0.1**	104.010	7.64×10^{14}	51.651	4.96×10^{9}
	0.2	107.049	9.89×10^{14}	64.784	6.23×10^{9}
	0.3	113.301	2.46×10^{15}	67.362	9.54×10^{10}
	0.4	113.877	1.68×10^{15}	67.362	2.01×10^{10}
	0.5	110.991	5.78×10^{14}	51.629	2.05×10^{9}
	0.6	108.271	2.35×10^{14}	47.601	7.48×10^{8}
	0.7	108.462	5.17×10^{13}	42.790	3.68×10^{8}
	0.8	109.946	2.07×10^{14}	42.790	2.25×10^{8}
	0.9	107.517	1.02×10^{14}	47.260	5.01×10^{8}
	Avg	109.269	7.85×10^{14}	53.692	1.45×10^{10}
STR	**0.1**	108.604	7.58×10^{9}	108.311	6.98×10^{9}
	0.2	111.018	8.06×10^{9}	111.291	8.28×10^{9}
	0.3	114.394	1.00×10^{10}	114.092	8.28×10^{9}
	0.4	122.172	2.83×10^{10}	122.118	2.72×10^{10}
	0.5	134.955	2.30×10^{11}	137.394	3.67×10^{11}
	0.6	145.072	1.18×10^{12}	148.686	2.35×10^{12}
	0.7	147.367	1.32×10^{12}	151.363	2.81×10^{12}
	0.8	148.308	1.33×10^{12}	152.829	2.62×10^{12}
	0.9	153.358	1.99×10^{12}	157.977	4.64×10^{12}
	Avg	131.694	6.78×10^{11}	133.784	1.43×10^{12}

variables, particularly in STR, indicate that the artificial neural network model does not sufficiently include the frequency of molecule collisions or the intricacy of the experimental process (V. K. Kumar, Hallad, and Panwar 2024; Padma et al. 2024).

For the KAS and STR methods, the ANN27 model predicts activation energy (Ea) with low errors (1.66% and 1.59%, respectively). However, it struggles with pre-exponential factor (A) predictions across all methods, displaying large errors (e.g., 2.24×10^{15} % for KAS) and significantly underestimates Ea for the FWO method (50.86% error). These differences, which are shown in Table 6, demonstrate the model's

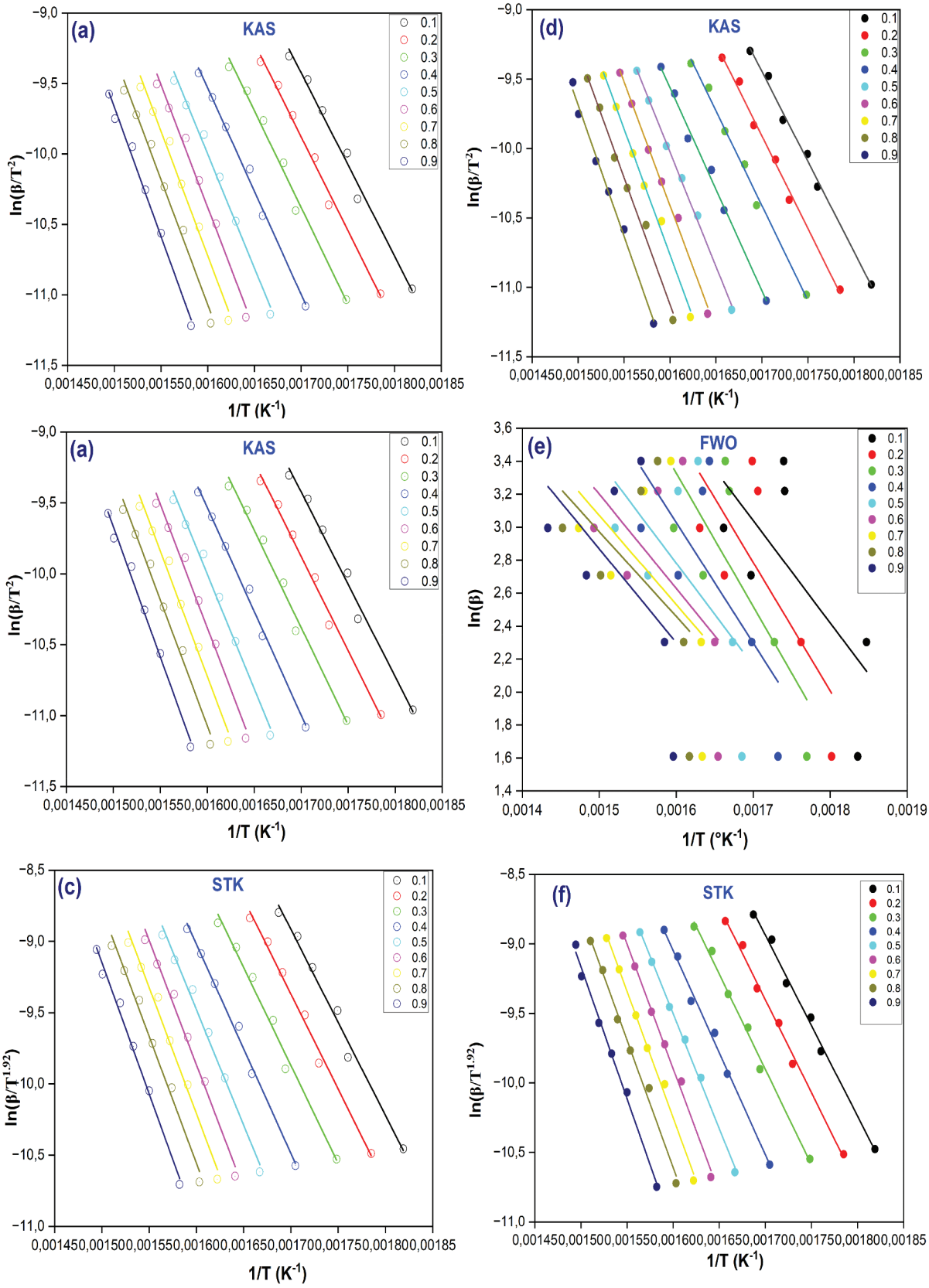

Figure 10. Estimation of the activation energy (Ea) of DDFs using the FWO, Kas, and STR techniques, utilizing TGA experimental data and optimum ANN-predicted model data.

Table 6. Comparison of experimental and ANN-Predicted average activation energy (Ea) and Pre-exponential factor (a) with error analysis for Kas, FWO, and STR methods.

Methods	Data Type	Avg Ea (kJ/mol)	Abs Error Ea (kJ/mol)	% Error Ea	Avg A (s^{-1})	Abs Error A (s^{-1})	% Error A
KAS	Experimental	131.244	2.176	1.66%	3.53×10^{12}	7.92×10^{25}	2.24×10^{15} %
	Predicted (ANN27)	133.420			7.92×10^{25}		
FWO	Experimental	109.269	55.577	50.86%	7.85×10^{14}	7.85×10^{14}	5.41×10^{6} %
	Predicted (ANN27)	53.692			1.45×10^{10}		
STR	Experimental	131.694	2.090	1.59%	6.78×10^{11}	7.52×10^{11}	110.91%
	Predicted (ANN27)	133.784			1.43×10^{12}		

Table 7. Estimation of thermodynamic parameters values using three model-free methods for experimental and optimal ANN-predicted model data.

		Experimental data			Optimal ANN-predicted data		
Methods	α	ΔH (kJ/mol)	ΔG (kJ/mol)	ΔS (kJ/mol)	ΔH (kJ/mol)	ΔG (kJ/mol)	ΔS (J/mol*K)
KAS	0.1	95.91	105.91	−13.34	73.495	104.345	−51.29
	0.2	98.3	108.3	−14.27	76.474	107.324	−50.35
	0.3	101.68	111.68	−13.33	79.255	110.105	−51.30
	0.4	109.429	119.429	−13.73	87.262	118.112	−50.89
	0.5	122.215	132.215	−17.82	102.632	133.482	−46.80
	0.6	132.223	142.223	−19.78	113.878	144.728	−44.84
	0.7	134.51	144.51	−20.41	116.562	147.412	−44.22
	0.8	135.434	145.434	−21.28	118.033	148.883	−43.35
	0.9	140.434	150.434	−21.44	123.135	153.985	−43.19
	Avg	118.90	128.90	−17.27	98.96	129.82	−47.36
FWO	0.1	91.67	101.67	69.01	17.201	48.051	−133.65
	0.2	94.709	104.70	53.04	30.334	61.184	−117.68
	0.3	100.961	110.96	58.86	32.912	63.762	−123.49
	0.4	101.537	111.53	59.77	32.912	63.762	−124.40
	0.5	98.651	108.65	80.098	17.179	48.029	−144.73
	0.6	95.931	105.93	82.16	13.151	44.001	−146.80
	0.7	96.122	106.12	90.08	8.34	39.19	−154.71
	0.8	97.606	107.60	92.43	8.34	39.19	−157.06
	0.9	95.177	105.17	81.55	12.81	43.66	−146.15
	Avg	96.92	106.92	74.11	19.24	50.09	−138.74
STR	0.1	91.67	101.67	−20.67	73.86	104.71	−44.00
	0.2	94.71	104.71	−20.54	76.84	107.69	−44.09
	0.3	100.96	110.96	−15.08	79.64	110.49	−49.55
	0.4	101.57	111.53	−26.86	87.66	118.52	−37.76
	0.5	98.65	108.65	−55.60	102.94	133.79	−9.03
	0.6	95.93	105.93	−77.77	114.23	145.08	13.14
	0.7	96.12	106.12	−81.71	116.91	147.76	17.07
	0.8	97.60	107.60	−81.68	118.38	149.23	17.04
	0.9	95.17	105.17	−93.67	123.52	154.37	29.03
	Avg	96.93	106.93	−52.62	99.33	130.18	−12.01

dependability for Ea in particular situations but point to its inability to capture A and FWO kinetics. This suggests that improved training data or network architecture are required to improve the predictive accuracy for *Dracaena Draco* fiber pyrolysis.

Thermodynamic analysis

In Table 7, the thermodynamic parameters entropy change (ΔS), enthalpy change (ΔH), and Gibbs free energy change (ΔG) between experimental and ANN27-predicted data are evaluated using three model-free methods data (FWO, KAS, and STR).

The KAS method demonstrates a strong correlation between the experimental and ANN27-modeled thermodynamic parameters for the pyrolysis process. The experimental values for enthalpy change (ΔH) range from 95.91 to 140.434 kJ/mol (average 118.90 kJ/mol), while the ANN27 predictions are somewhat lower, ranging from 73.495 to 123.135 kJ/mol (average 98.96 kJ/mol). This indicates the accuracy of the model. Both the experimental and ANN27 models exhibit a substantial overestimation of the Gibbs free energy (ΔG) values, with averages of 128.90 kJ/mol (experimental) and 129.82 kJ/mol (ANN27). These findings indicate a slight overestimation of the lack of spontaneity in the reactions. The entropy change (ΔS) values exhibited an experimental range of −13.34 to

Table 8. Average thermodynamic parameters (ΔH, ΔG, ΔS) and error analysis for experimental and ANN27-predicted data using Kas, FWO, and STR methods.

Methods	Data Type	Avg ΔH (kJ/mol)	Abs Error ΔH	% Error ΔH	Avg ΔG (kJ/mol)	Abs Error ΔG	% Error ΔG	Avg ΔS (J/mol·K)	Abs Error ΔS	% Error ΔS
KAS	Experimental	118.90	19.94	16.77%	128.90	0.92	0.71%	−17.27	30.09	174.23%
	Predicted (ANN27)	98.96			129.82			−47.36		
FWO	Experimental	96.92	77.68	80.15%	106.92	56.83	53.15%	74.11	212.85	287.23%
	Predicted (ANN27)	19.24			50.09			−138.74		
STR	Experimental	96.93	2.40	2.48%	106.93	23.25	21.74%	−52.62	40.61	77.17%
	Predicted (ANN27)	99.33			130.18			−12.01		

−21.44 J/mol.K, with an average of −17.27 J/mol.K. In contrast, the range of ANN27 was −43.19 to −51.30 J/mol.K, with an average of −47.36 J/mol.K. This indicates that the model may somewhat overestimate the disorder of the system during pyrolysis.

Empirical enthalpy change (ΔH) values obtained using the FWO technique range from 91.67 to 101.537 kJ/mol, with an average of 96.92 kJ/mol. Nevertheless, the ANN27 model considerably overestimates the amount of ΔH, forecasting values between 8.34 and 32.912 kJ/mol, with an average of 19.24 kJ/mol. This suggests a larger anticipated energy need for pyrolysis. The experimental results show an average ΔG value of 106.92 kJ/mol. However, the predictions made by ANN27 are somewhat lower at 50.09 kJ/mol, suggesting a less advantageous spontaneous reaction. The entropy change (ΔS) values exhibit greater consistency between experimental data, which range from 53.04 to 92.43 J/mol.K (with an average of 74.11 J/mol.K), and ANN27 predictions, which range from −117.68 to −157.06 J/mol.K (with an average of −138.74 J/mol.K). This result suggests a minor inaccuracy in the model's estimation, but nevertheless indicates a satisfactory level of accuracy in predicting entropy changes.

The experimental enthalpy change (ΔH) values obtained by the STR approach vary between 91.67 and 101.57 kJ/mol, with an average of 96.93 kJ/mol. By contrast, the ANN27 model slightly above the threshold of ΔH, forecasting values ranging from 73.86 to 123.52 kJ/mol, with an average of 169.1899.33 kJ/mol. These findings indicate that the procedure will need a greater amount of energy than expected. The experimental data of 106.93 kJ/mol and the predictions made by ANN27 of 130.18 kJ/mol demonstrate a satisfactory level of precision in the determination of Gibbs free energy (ΔG) values. However, the entropy change (ΔS) exhibits notable inconsistencies, as observed values vary from −15.08 to −93.67 J/mol.K (average −52.62 J/mol.K) and ANN27 predictions vary from −9.03 to 29.03 J/mol.K (average −12.01 J/mol.K). This indicates a possible constraint of the ANN27 model in effectively forecasting entropy changes, possibly attributed to the challenges associated with the thermal degradation behavior of DDFs.

The predictive accuracy of the ANN27 model in determining enthalpy (ΔH) and Gibbs free energy (ΔG) is in agreement with experimental data. Nevertheless, it somewhat overstates these values, suggesting a cautious strategy by forecasting greater energy demands and fewer desirable spontaneous behaviors. Nevertheless, discrepancies in predicting the decrease in entropy (ΔS), particularly in the STR approach, indicate that the model may need additional improvement to accurately depict the complexities of the DDF pyrolysis cycle. In general, the ANN27 model is a valuable prediction tool, however its performance differs depending on the parameters input. Conducting additional calibration using diverse experimental data is expected to enhance the reliability and precision of forecasting thermodynamic properties during DDF pyrolysis (Hernández-Rizo, Larios-Durán, and Bárcena-Soto 2023).

With error analysis, Table 8 compares the thermodynamic parameters (ΔH, ΔG, and ΔS) for the pyrolysis of *Dracaena Draco* fiber using the KAS, FWO, and STR techniques. Due to limited experimental values, the ANN27 model struggles with ΔS (77.17–287.23% error) across all methods and underestimates ΔH (16.77–80.15%) and ΔG (21.74–53.15%) for FWO and STR. It also accurately predicts ΔG for KAS (0.71% error) and ΔH for STR (2.48% error). Although useful for some parameters, ANN27 is a useful yet adaptable tool for pyrolysis optimization; higher entropy predictions and FWO alignment require enhancements in training data or design.

Conclusion

Using thermogravimetric analysis (TGA) data, this study effectively created and refined an artificial neural network (ANN) model to forecast the thermal degradation behavior of *Dracaena Draco* lignocellulosic fibers. The ANN's precise representation of pyrolysis behavior, curve shapes, and component degradation patterns closely matched experimental findings confirmed by model-free techniques like Kissinger-Akahira-Sunose (KAS), Flynn-Wall-Ozawa (FWO), and Starink. These results show how well the model predicts thermal deterioration, providing a trustworthy instrument for materials science studies. The potential uses of this work, such as identifying dissociation energies, improving processing conditions, and expanding our understanding of the mechanisms underlying lignocellulosic fiber degradation, make it significant. This study adds to the expanding application of machine learning in comprehending complicated material behaviors, especially in the context of sustainable biomaterials, by incorporating ANN approaches.

In the future, this method might be improved by investigating different ANN structures or applied to other lignocellulosic fibers, opening the door for further significant developments in material optimization and thermal stability analysis.

Highlights

- The study employed TGA to characterize the thermal decomposition of DDFs.
- A model of an ANN was successfully created and fine-tuned to accurately forecast the thermal deterioration behavior of DDFs.
- The ANN model effectively captured the pyrolysis behavior, curve shapes, and component degradation patterns observed in the experimental data.
- This method has the potential to be used for optimizing processing conditions, determining dissociation energies, and gaining further insights into the degradation mechanisms of DDFs.

Disclosure statement

No potential conflict of interest was reported by the author(s).

ORCID

Ahmed Belaadi http://orcid.org/0000-0002-6059-3974

Nomenclature and abbreviations

DDFs	Dracaena Draco fibers
TGA	thermogravimetric analysis
DTG	Differential thermogravimetry
β	Heating rate (°C/min)
MBE	mean bias error
RMSE	root mean square error
R^2	Coefficient of correlation
MAE	mean absolute error
ANN	artificial neural network

References

Ali, I., R. Tariq, S. R. Naqvi, A. H. Khoja, M. T. Mehran, M. Naqvi, et N. Gao. 2021. "Kinetic and Thermodynamic Analyses of Dried Oily Sludge Pyrolysis." *Journal of the Energy Institute* 95:30–40. https://doi.org/10.1016/j.joei.2020.12.002.

Alongi, J., R. A. Carletto, A. Di Blasio, F. Carosio, and F. Bosco, et G. Malucelli. 2013. "DNA: a novel, green, natural flame retardant and suppressant for cotton." *Journal of Materials Chemistry A* 1 (15): 4779–4785. https://doi.org/10.1039/c3ta00107e.

Alongi, J. et G. Malucelli. 2015. *Reactions and Mechanisms in Thermal Analysis of Advanced Materials*. Tiwari, A., Raj, B., Eds. Hoboken, NJ, USA: Wiley Scrivener Publisher.

Altıntaş, O., M. Aksoy, E. Ünal, and O. Akgöl, et M. Karaaslan. 2019. "Artificial Neural Network Approach for Locomotive Maintenance by Monitoring Dielectric Properties of Engine Lubricant." *Measurement* 145:678–686. https://doi.org/10.1016/j.measurement.2019.05.087.

Aquino, E. M. F., L. P. S. Sarmento, W. Oliveira, et R. V. Silva. janv. 2007. "Moisture Effect on Degradation of jute/Glass Hybrid Composites." *Journal of Reinforced Plastics & Composites* 26 (2): 219–233. https://doi.org/10.1177/0731684407070030.

Basak, S. et S. W. Ali. 2022. "Sodium Lignin Sulfonate (SLS) and Pomegranate Rind Extracts (PRE) Bio-Macro-Molecule: A Novel Composition for Making Fire Resistant Cellulose Polymer." *Combustion Science and Technology* 194 (15): 3206–3224. nov. https://doi.org/10.1080/00102202.2021.1922397.

Basak, S., A. S. M. Raja, S. Saxena, et P. G. Patil. 2021. "Tannin Based Polyphenolic Bio-Macromolecules: Creating a New Era Towards Sustainable Flame Retardancy of Polymers." *Polymer Degradation & Stability* 189:109603. https://doi.org/10.1016/j.polymdegradstab.2021.109603.

Bednaya, T. A. et S. P. Konovalenko. 2018. "Development of a Neural Network Model for Predicting the Physical and Chemical Properties of Materials from the Technological Parameters of Their Formation." *IOP Conference Series: Materials Science and Engineering*, 012086. IOP Publishing. https://iopscience.iop.org/article/10.1088/1757-899X/447/1/012086/meta.

Bhowmick, M., S. Basak, et K. K. Samanta. 2022. "Ramie Degum Liquor: Wastage Bio-Macromolecule for Making Thermally Stable Functionalize Polyester Fabric." *Polymer Degradation & Stability* 200:109959. https://doi.org/10.1016/j.polymdegradstab.2022.109959.

Castro, J. D. S., E. G. P. da Silva, et C. F. Virgens. 2020. "Evaluation of Models to Predict the Influence of Chemical Pretreatment on the Peels of Nephelium Lappaceum L. Based on Pyrolysis Kinetic Parameters Obtained Using a Combined Fraser-Suzuki Function and Friedman's Isoconversional Method." *Journal of Analytical and Applied Pyrolysis* 149:104827. https://doi.org/10.1016/j.jaap.2020.104827.

Chen, D., A. Gao, K. Cen, J. Zhang, X. Cao, et Z. Ma. 2018. "Investigation of Biomass Torrefaction Based on Three Major Components: Hemicellulose, Cellulose, and Lignin." *Energy Conversion and Management* 169:228–237. https://doi.org/10.1016/j.enconman.2018.05.063.

Chen, W.-H., C.-W. Wang, H. C. Ong, P. L. Show, et T.-H. Hsieh. 2019. "TorrefactiTorrefactiOn, Pyrolysis and Two-Stage Thermodegradation of Hemicellulose, Cellulose and Lignin." *Fuel* 258:116168. https://doi.org/10.1016/j.fuel.2019.116168.

Conesa, J. A., J. A. Caballero, et J. A. Reyes-Labarta. 2004. "Artificial Neural Network for Modelling Thermal Decompositions." *Journal of Analytical and Applied Pyrolysis* 71 (1): 343–352. https://doi.org/10.1016/S0165-2370(03)00093-7.

Debnath, S., M. M. Reddy, et Q. S. Yi. 2016. "Influence of Cutting Fluid Conditions and Cutting Parameters on Surface Roughness and Tool Wear in Turning Process Using Taguchi Method." *Measurement* 78:111–119. https://doi.org/10.1016/j.measurement.2015.09.011.

Ding, Z., Z. Chen, J. Liu, F. Evrendilek, Y. He, et W. Xie. 2022. "Co-combustion, Life-Cycle Circularity, and Artificial Intelligence-Based Multi-Objective Optimization of Two Plastics and Textile Dyeing Sludge." *Journal of Hazardous Materials* 426 (December 2021): 128069. https://doi.org/10.1016/j.jhazmat.2021.128069.

Fu, J., X. Wu, J. Liu, F. Evrendilek, T. Chen, W. Xie, W. Xu, et Y. He. 2023. "Co-Circularity of Spent Coffee Grounds and Polyethylene via Co-Pyrolysis: Characteristics, Kinetics, and Products." *Fuel* 337 (December 2022): 127061. https://doi.org/10.1016/j.fuel.2022.127061.

Giridharan, R. 2019. "Preparation and Property Evaluation of glass/Ramie Fibers Reinforced Epoxy Hybrid Composites." *Composites Part B Engineering* 167:342–345. https://doi.org/10.1016/j.compositesb.2018.12.049.

Hadou, A., A. Belaadi, H. Alshahrani, et M. K. A. Khan. févr. 2024. "Extraction and Characterization of Novel Cellulose Fibers from Dracaena Draco Plant." *Materials Chemistry and Physics* 313:128790. https://doi.org/10.1016/j.matchemphys.2023.128790.

Hadou, A., A. Belaadi, I. M. H. Alshaikh, et D. Ghernaout. déc. 2024. "Pyrolysis Features of Dracaena Draco Lignocellulosic Fibers: Kinetic and Thermodynamic Analysis at Various Heating Rates Through Coats-Redfern Method." *Case Studies in Thermal Engineering* 64:105406. https://doi.org/10.1016/j.csite.2024.105406.

Hernández-Rizo, S. G., E. R. Larios-Durán, et M. Bárcena-Soto. 2023. "Frequency Response of Gibbs Free Energy and Enthalpy Changes of Electrochemical Systems Analyzed as Thermometric Transfer Functions." *Journal of Solid State Electrochemistry* 27 (11): 3177–3188. https://doi.org/10.1007/s10008-023-05553-3.

Huang, H., T. Yang, F. Lai, et G. Wu. 2017. "Co-Pyrolysis of Sewage Sludge and Sawdust/Rice Straw for the Production of Biochar." *Journal of Analytical and Applied Pyrolysis* 125:61–68. https://doi.org/10.1016/j.jaap.2017.04.018.

Jiang, C., W. Zhou, H. Bi, Z. Ni, H. Sun, et Q. Lin. 2022. "Co-Pyrolysis of Coal Slime and Cattle Manure by TG–FTIR–MS and Artificial Neural Network Modeling: Pyrolysis behavior, Kinetics, Gas Emission Characteristics." *Energy* 247:123203. https://doi.org/10.1016/j.energy.2022.123203.

John, M. J. et S. Thomas. févr. 2008. "Biofibres and Biocomposites." *Carbohydrate Polymers* 71 (3): 343–364. https://doi.org/10.1016/j.carbpol.2007.05.040.

Kozlov, A. N., D. A. Svishchev, G. I. Khudiakova, et A. F. Ryzhkov. 2017. "A Kinetic Analysis of the Thermochemical Conversion of Solid Fuels (A Review)." *Solid Fuel Chemistry* 51 (4): 205–213. https://doi.org/10.3103/S0361521917040061.

Kumar, M., D. Rai, G. Bhardwaj, S. N. Upadhyay, et P. K. Mishra. 2021. "Pyrolysis of Peanut Shell: Kinetic Analysis and Optimization of Thermal Degradation Process." *Industrial Crops and Products* 174:114128. https://doi.org/10.1016/j.indcrop.2021.114128.

Kumar, V. K., S. C. Hallad, et N. L. Panwar. 2024. "Thermogravimetric Pyrolysis Investigation of Pistachio Shell for Its Potential of Thermal Properties, Kinetics and Thermodynamics." *Discover Energy* 4 (1). https://doi.org/10.1007/s43937-024-00030-y.

Lazzari, L. K., V. B. Zampieri, R. M. Neves, M. Zanini, A. J. Zattera, et C. Baldasso. janv. 2019. "A Study on Adsorption Isotherm and Kinetics of Petroleum by Cellulose Cryogels." *Cellulose* 26 (2): 1231–1246. https://doi.org/10.1007/s10570-018-2111-x.

Lopes, F. C. R. et K. Tannous. 2020. "Coconut Fiber Pyrolysis Decomposition Kinetics Applying Single-And Multi-Step Reaction Models." *Thermochimica Acta* 691:178714. https://doi.org/10.1016/j.tca.2020.178714.

Mishra, A., S. Nanda, M. Ranjan Parida, P. K. Jena, S. K. Dwibedi, S. Manjari Samantaray, D. Samantaray, M. K. Mohanty, et M. Dash. 2023. "A Comparative Study on Pyrolysis Kinetics and Thermodynamic Parameters of Little Millet and Sunflower Stems Biomass Using Thermogravimetric Analysis." *Bioresource Technology* 367 (November 2022): 128231. https://doi.org/10.1016/j.biortech.2022.128231.

Moayedi, H. et A. Rezaei. 2019. "An Artificial Neural Network Approach for Under-Reamed Piles Subjected to Uplift Forces in Dry Sand." *Neural Computing & Applications* 31 (2): 327–336. févr. https://doi.org/10.1007/s00521-017-2990-z.

Monticeli, F. M., J. H. S. Almeida, R. M. Neves, F. G. Ornaghi, et H. L. Ornaghi. 2020. "On the 3D Void Formation of Hybrid Carbon/Glass Fiber Composite Laminates: A Statistical Approach." *Composites Part A, Applied Science and Manufacturing* 137:106036. https://doi.org/10.1016/j.compositesa.2020.106036.

Monticeli, F. M., R. M. Neves, et H. L. Ornaghi Júnior. 2021. "Using an Artificial Neural Network (ANN) for Prediction of Thermal Degradation from Kinetics Parameters of Vegetable Fibers." *Cellulose* 28 (4): 1961–1971. mars. https://doi.org/10.1007/s10570-021-03684-2.

Motta Neves, R., K. Silveira Lopes, M. G. V. Zimmermann, M. Poletto, et A. J. Zattera. 2020. "Cellulose Nanowhiskers Extracted from tempo-Oxidized Curaua Fibers." *Journal of Natural Fibers* 17 (9): 1355–1365. sept. https://doi.org/10.1080/15440478.2019.1568346.

Moukhina, E. 2012. "Determination of Kinetic Mechanisms for Reactions Measured with Thermoanalytical Instruments." *Journal of Thermal Analysis and Calorimetry* 109 (3): 1203–1214. https://doi.org/10.1007/s10973-012-2406-3.

Nasri, K. et L. Toubal. 2024. "Artificial Neural Network Approach for Assessing Mechanical Properties and Impact Performance of Natural-Fiber Composites Exposed to UV Radiation »." *Polymers* 16 (4): 538. https://doi.org/10.3390/polym16040538.

Neves, R. M., K. S. Lopes, M. V. G. Zimmermann, M. Poletto, et A. J. Zattera. 2019. "Characterization of Polystyrene Nanocomposites and Expanded Nanocomposites Reinforced with Cellulose Nanofibers and Nanocrystals." *Cellulose* 26 (7): 4417–4429. mai. https://doi.org/10.1007/s10570-019-02392-2.

Ornaghi, H. L., R. M. Neves, et F. M. Monticeli. 2021. "Application of the Artificial Neural Network (ANN) Approach for Prediction of the Kinetic Parameters of Lignocellulosic Fibers." *Textiles* 1 (2): 258–267. https://doi.org/10.3390/textiles1020013.

Ornaghi, H. L., F. G. Ornaghi, R. M. Neves, F. Monticeli, et O. Bianchi. 2020. "Mechanisms Involved in Thermal Degradation of Lignocellulosic Fibers: A Survey Based on Chemical Composition." *Cellulose* 27 (9): 4949–4961. juin. https://doi.org/10.1007/s10570-020-03132-7.

Ornaghi, H. L., M. Poletto, A. J. Zattera, et S. C. Amico. févr. 2014. "Correlation of the Thermal Stability and the Decomposition Kinetics of Six Different Vegetal Fibers." *Cellulose* 21 (1): 177–188. https://doi.org/10.1007/s10570-013-0094-1.

Padma, D. V., K. R. Kumar, S. V. A. R. Sastry, et P. Barmavatu. 2024. "Studies on Thermal Degradation Kinetics and Machine Learning Modeling of Hydrochar Produced from Hydrothermal Carbonization of Municipal Sewage Sludge and Key Lime Peel." *Biomass Conversion and Biorefinery*. https://doi.org/10.1007/s13399-024-05749-1.

Pang, S. 2019. "Advances in Thermochemical Conversion of Woody Biomass to Energy, Fuels and Chemicals." *Biotechnology Advances* 37 (4): 589–597. https://doi.org/10.1016/j.biotechadv.2018.11.004.

Pathak, U., S. Kumari, A. Kumar, et T. Mandal. 2020. "Process Parametric Optimization Toward Augmentation of Silica Yield Using Taguchi Technique and Artificial Neural Network Approach." *Energy, Ecology and Environment* 5 (4): 294–312. août. https://doi.org/10.1007/s40974-020-00152-8.

Poletto, M., H. L. Ornaghi Junior, et A. J. Zattera. 2014. "Native Cellulose: Structure, Characterization and Thermal Properties." *Materials* 7 (9): 6105–6119. https://doi.org/10.3390/ma7096105.

Proskurina, S., M. Junginger, J. Heinimö, B. Tekinel, et E. Vakkilainen. 2019. "Global Biomass Trade for Energy—Part 2: Production and Trade Streams of Wood Pellets, Liquid Biofuels, Charcoal, Industrial Roundwood and Emerging Energy Biomass." *Biofuels, Bioproducts and Biorefining* 13 (2): 371–387. mars. https://doi.org/10.1002/bbb.1858.

Sánchez-Jiménez, P. E., L. A. Pérez-Maqueda, A. Perejón, et J. M. Criado. 2009. "Combined Kinetic Analysis of Thermal Degradation of Polymeric Materials Under Any Thermal Pathway." *Polymer Degradation & Stability* 94 (11): 2079–2085. https://doi.org/10.1016/j.polymdegradstab.2009.07.006.

Sunphorka, S., B. Chalermsinsuwan, et P. Piumsomboon. 2017. "Artificial Neural Network Model for the Prediction of Kinetic Parameters of Biomass Pyrolysis from Its Constituents." *Fuel* 193:142–158. https://doi.org/10.1016/j.fuel.2016.12.046.

Tabal, A., A. Barakat, A. Aboulkas, et K. El Harfi. 2021. "Pyrolysis of Ficus Nitida Wood: Determination of Kinetic and Thermodynamic Parameters." *Fuel* 283 (May 2020): 119253. https://doi.org/10.1016/j.fuel.2020.119253.

Turco, C., M. F. Funari, E. Teixeira, et R. Mateus. déc. 2021. "Artificial Neural Networks to Predict the Mechanical Properties of Natural fibre-Reinforced Compressed Earth Blocks (CEBs)." *Fibers* 9 (12): Art. no 12. https://doi.org/10.3390/fib9120078.

Uzuner, S. et D. Çekmecelioğlu. 2016. "Comparison of Artificial Neural Networks (ANN) and Adaptive Neuro-Fuzzy Inference System (ANFIS) Models in Simulating Polygalacturonase Production." Consulté le: 29 juin 2024. Disponible sur: https://open.metu.edu.tr/handle/11511/33030.

Vyazovkin, S. 2020. "Kissinger Method in Kinetics of Materials: Things to Beware and Be Aware of." *Molecules* 25 (12): 2813. https://doi.org/10.3390/molecules25122813.

Wang, Y., S. Yang, G. Bao, et H. Wang. 2023. "Investigation of Tobacco Straw Pyrolysis: Three-Parallel Gaussian Reaction Modeling, Products Analysis and ANN Application." *Industrial Crops and Products* 200:116864. https://doi.org/10.1016/j.indcrop.2023.116864.

Wang, Y., S. Yang, G. Bao, et H. Wang. 2024. "Pyrolytic Characteristics of Abutilon Stalk Waste Using tg-Ftir, py-Gc/ms, and Artificial Neural Networks: Kinetics, Thermodynamics, and Gaseous Products Distribution." *Journal of Analytical and Applied Pyrolysis* 178:106403. https://doi.org/10.1016/j.jaap.2024.106403.

Xiaowei, Z. 2015. "Critical Review of the Global Chemical Kinetics of Cellulose Thermal Decomposition."

Yao, F., Q. Wu, Y. Lei, W. Guo, et Y. Xu. 2008. "Thermal Decomposition Kinetics of Natural Fibers: Activation Energy with Dynamic Thermogravimetric Analysis." *Polymer Degradation & Stability* 93 (1): 90–98. https://doi.org/10.1016/j.polymdegradstab.2007.10.012.

Yeo, J. Y., B. L. F. Chin, J. K. Tan, et Y. S. Loh. 2019. "Comparative Studies on the Pyrolysis of Cellulose, Hemicellulose, and Lignin Based on Combined Kinetics." *Journal of the Energy Institute* 92 (1): 27–37. https://doi.org/10.1016/j.joei.2017.12.003.

Zanchet, A., R. Demori, F. D. B. De Sousa, H. L. Ornaghi, L. S. A. Schiavo, et C. H. Scuracchio. 2019. "Sugar Cane as an Alternative Green Activator to Conventional Vulcanization Additives in Natural Rubber Compounds: Thermal Degradation Study." *Journal of Cleaner Production* 207:248–260. https://doi.org/10.1016/j.jclepro.2018.09.203.

Zhang, W., J. Zhang, Y. Ding, Q. He, K. Lu, et H. Chen. 2021. "Pyrolysis Kinetics and Reaction Mechanism of Expandable Polystyrene by Multiple Kinetics Methods." *Journal of Cleaner Production* 285:125042. https://doi.org/10.1016/j.jclepro.2020.125042.

Zhang, Z. et K. Friedrich. 2003. "Artificial Neural Networks Applied to Polymer Composites: A Review." *Composites Science and Technology* 63 (14): 2029–2044. https://doi.org/10.1016/S0266-3538(03)00106-4.